SACLANT UNDERSEA RESEARCH CENTRE

MEMORANDUM

Development of barotropic models for the GIN Sea

S. Piacsek and
P. van Meurs

March 1991

Page count for SM-242
(excluding covers)

Pages	Total
i–vi	6
1–48	48
	54

SACLANT Undersea Research Centre
Viale San Bartolomeo 400
19026 San Bartolomeo (SP), Italy

tel: 0187 540 111
fax: 0187 524 600
telex: 271148 SACENT I

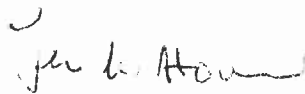NORTH ATLANTIC TREATY ORGANIZATION

SACLANTCEN SM-242

Development of barotropic
models for the GIN Sea

S. Piacsek and P. van Meurs

Issued by:
Underwater Research Division

J.M. Hovem
Division Chief

intentionally blank page

SACLANTCEN SM-242

**Development of barotropic models
for the GIN Sea**

S. Piacsek and P. van Meurs

Executive Summary: In the past, ASW operations have relied heavily on climatological hydrographic data to compute sound-velocity profiles. However, available data from satellites and AXBT flight patterns have revealed the gross inadequacy of climatology to represent the actual temperature and salinity over wide areas in strong frontal regions. To overcome this inadequacy, frequent synoptic (real-time) data collections must be carried out to update the sound-velocity information.

Ocean models complement data collection by predicting the currents that change the thermal structure between times of data collection. In this way, numerical ocean models supply acoustic velocity information between times of observations and in regions not accessible to data-gathering. Under adverse conditions (e.g. bad weather, enemy fire) one must rely primarily on such models to accurately estimate acoustic propagation conditions for ASW operations.

Research during the last few decades have greatly advanced the understanding of oceanic fronts, and their structures and variabilities. One important conclusion from this work is that oceanic fronts are frequently associated with strong currents. For example, the Iceland–Faeroe Front in the Greenland–Iceland–Norwegian (GIN) Seas is formed at the intersection of the North Atlantic and the East Iceland Currents. Thus the prediction of ocean currents is crucial to a successful prediction of the thermal structure in frontal regions.

This study is a first step in the general prediction of currents in the GIN Sea region. It predicts the total mass transport represented by the vertically-averaged currents (called barotropic currents by oceanographers). This first report on the study presents the model formulation, the testing of the impact of various bottom and horizontal friction values on the resulting circulation, and a preliminary examination of the seasonal variation of the monthly mean barotropic circulation in the GIN Sea.

intentionally blank page

**Development of barotropic models
for the GIN Sea**

S. Piacsek and P. van Meurs

Abstract: Barotropic ocean models are developed for deep oceans, with arbitrary topography and basin geometry, on a sphere. A special adaptation is made for the Greenland–Iceland–Norwegian (GIN) Seas with closed lateral boundaries. The models are tested for conservation, accuracy and physical soundness at successive stages of their development. Various results obtained with an explicit version of the model with closed boundaries are presented. These include runs with a flat bottom and GIN topography, using monthly-averaged wind forcing.

Keywords: barotropic ocean models ∘ circulation ∘ currents ∘ GIN Sea ∘ propagation conditions ∘ satellite remote sensing ∘ sound-velocity profiles

Contents

1
Introduction

The SACLANTCEN modelling programme of the Greenland–Iceland–Norwegian (GIN) Sea has two purposes:

(a) To provide the general circulation and thermodynamic state of the GIN Sea that is consistent with all available hydrographic/atmospheric forcing data.

(b) To provide the initial background environment and the prediction models for real-time nowcasts and forecasts for any part of the GIN Sea.

As we know from previous modelling efforts and our knowledge of the physical processes of the ocean, to build a 'universal' ocean model that can treat accurately phenomena on all spatial and temporal scales in the various ocean basins of the world is difficult. This difficulty is due both to finite computer size and speed, and to an imperfect description of the physical processes, such as turbulence. Thus ocean modelling efforts have diversified into different classes; some are concerned only with the turbulent surface boundary layers, some with continental shelves, and many with the meso-scale eddy-resolving circulation in a given part of, or a whole, ocean basin. World ocean models of high resolution are nearing testing. Similarly, models that aim to give real-time nowcasts and forecasts from objectively analyzed density fields and model-predicted atmospheric forcing have only recently begun extensive testing using real-time observations. Generally, these prediction models apply to a limited domain with open boundaries. They can predict only for a few days ahead unless observations made within the domain provide additional information at the boundaries.

Since the GIN Sea basin is relatively small as compared to ocean basins that have been successfully modelled, we can build a general circulation model that will treat both the thermodynamic and hydrodynamic aspects. This model can provide the general oceanographic background which the real-time forecast models need.

This memorandum describes several barotropic ocean models. In general, the types of ocean models that we need for our tasks in the GIN Sea are called baroclinic models, i.e. ocean models that describe the response of a variable density ocean to atmospheric momentum and heat forcing. All contain a barotropic component which represents the vertically-averaged component of the motion. Barotropic models are closely related to the classic shallow water models in which pressure depends only on depth, as given by the classic hydrostatic equation $p = \rho g z$, with ρ, the density of sea water, and g, the acceleration due to gravity, being constants. Such models

are used by engineers in tidal channels or by coastal and estuarine investigators in situations where the forcing due to density variations is minor or negligible. However, important differences exist between shallow water and barotropic models in general. Firstly, true barotropic models also include terms that represent the contributions from the vertically-averaged pressure gradients associated with the density variations. Secondly, difficulties arise in the computations of energy transformations caused by the nonlinear processes because the average of the squares is not equal to the square of the average. Even though the momentum equations correctly represent the evolution of the mean momentum of the system when the flow varies with depth, the nonlinear terms and the derived energy equations will err significantly if the flow contains strong vertical variations. This is especially true if these velocity reversals occur in the eddy-dominated regions of the ocean containing much of the energy of the flow. Consideration must be given to additional terms usually neglected in true shallow water situations, where the flow tends to be vertically homogeneous.

Why is barotropic modelling done at all except in conjunction with baroclinic modelling? Three reasons are immediately apparent:

1. Probably the most important reason is that the free surface elevation couples directly to the barotropic mode. The associated surface gravity waves, with their fast propagation velocities, can cause great problems for the numerical computations. Hence studying the efficiency and accuracy of the numerical techniques employed in a 2-D setting, is more cost-effective than in a 3-D baroclinic setting. Finding numerical schemes that can remove the impediment to taking large time-steps in an efficient ocean model is important.

   The point concerning the central role of the free surface in barotropic models becomes even more important when altimeter measurements of the sea surface elevation are used as part of the initialization/updating procedure for real-time prediction. This is because the information about the free surface elevation is first passed through the barotropic mode before its pressure effects are felt by the whole water column.

2. In certain oceanic regions, especially during the winter, deep convective mixing can occur; this mixing will tend to homogenize the density field over most of the depth range. Thus the barotropic part may represent a significant if not the dominant component of the total circulation. Using only a barotropic model can lead to useful insights into its patterns.

3. A final consideration – the models can supply the missing constant of integration for the well-known inverse ocean models, in which pressure gradients are balanced only by the Coriolis force. These inverse models offer a unique and fast way of computing the geostrophic (i.e. large-scale) currents when only the density field is known, as is often the case.

No specific barotropic modelling efforts have been performed for the GIN Sea so far. Such efforts have been made for the relatively shallow North Sea, or as a

component of a multi-layer baroclinic modelling effort [1,2,4]. A comprehensive review of many of the North Sea modelling efforts are presented in [5] and although most of the results are not directly applicable to the deep GIN Sea, the model equations, numerical techniques and the handling of the diffusion and bottom drag terms have served as a starting point for many of our considerations.

Aagaard [3] has computed the monthly-averaged winds for 1965 from pressure fields obtained from the Norwegian Meteorological Office. From the curl of these winds he has computed the Sverdrup transport in the GIN Sea, given by

$$V = (\nabla \times \tau)_z/\beta,$$

where $\nabla \times \tau$ is the wind stress, β is the latitudinal variation of the Coriolis force and the subscript z indicates that the axis of the curl vector is in the vertical direction. Such balance assumes a near-steady state and the non-divergence of the large-scale flow, and ignores topographic effects. The Sverdrup relation has been found to be very helpful in interpreting the large scale circulations of the Atlantic and Pacific basins. The mass transport isolines (streamlines) computed by Aagaard have corresponded to a cyclonic circulation over most of the GIN Sea area. This is consistent with the dominantly cyclonic nature of the annual and September mean winds prevailing in 1965 over the GIN Sea, and with the observed general surface circulation. We shall see later, however, that this does not apply to all years, nor to all seasons of the same year. Though dominantly cyclonic over the whole GIN Sea in most of 1983, during a large fraction of 1985, and particularly during 1987, the Greenland high has moved eastward, extending an anti-cyclonic wind pattern over most of the northwest quarter of the GIN Sea.

In order to reexamine Aagaard's conclusions in the presence of boundary inflows and topography, Creegan [1] has employed a 2-layer baroclinic numerical ocean model for the GIN Sea with an adjustable topography (i.e. it used a multiplication factor which made the bottom vary from flat to high relief topography). She has not isolated the barotropic component *per se*, but its behaviour can be deduced from the results of the combined calculations. We will discuss her results more fully in a comparison with the results of the present simulations in Sect. 3 and will note here only her main conclusions. She has performed both flat bottom and reduced-topography simulations, with or without boundary inflows; she found that topography has an overwhelming effect on the circulation. Without topography the circulation was found to reflect the vorticity pattern of the wind. With topography present the flow in general followed the f/H contours ($f = 2\Omega$, the Coriolis force; and $H(x,y)$, the depth) in each of the sub-basins of the GIN Sea, with the strongest flow in the Norwegian basin. She has also concluded that in general the observed circulation can not be explained without including the source-sink flows at the open boundaries.

2

Model description

2.1. PHYSICAL ASSUMPTIONS

We begin our model formulation with some assumptions. We assume a constant density ocean on a rotating sphere with a free surface. We assume the ocean to be shallow; thus the large horizontal/vertical aspect ratio allows us to use the hydrostatic approximation where we can neglect vertical accelerations. In the beginning we also assumed that the flow did not vary with depth, so that we can operate with a 2-D model. At some later stage of our barotropic modelling work, especially when it will be coupled to a baroclinic model, we will include the depth variations in order

(a) to obtain the correct formulation of the nonlinear terms,

(b) to include bottom and surface Ekman layers, and

(c) to handle the eventual coupling between the baroclinic and barotropic terms.

The geometry and bottom topography of the ocean basin has been taken through various stages of approximations until they have coincided reasonably well with the irregular geometry and topography of the GIN Sea. This is particularly useful, if not necessary, during the testing of the conservation properties and of the general accuracy of the numerical finite difference schemes. The smoothing scheme and the source of the topography is discussed in Subsect. 2.5. Similar considerations will apply to the atmospheric and boundary mass flux forcings, discussed in Subsect. 2.6.

We have proceeded to introduce the forcing functions through the following stages:

(a) closed boundaries, steady winds;

(b) extended boundaries, time-dependent winds;

(c) open boundaries, no winds; and

(d) open boundaries, time-dependent winds.

In this memorandum we present only the results for stage (a), closed boundaries and steady winds. Stages (b–d) will be discussed in later reports.

2.2. MODEL EQUATIONS

Assuming constant friction and starting with the general 3-D incompressible hydrodynamic equations, we can derive the equations for a constant density, hydrostatic ocean on a sphere (see Appendix A). The resultant equations are given by

$$
\mathrm{d}U/\,\mathrm{d}t = [fV + (U\tan\phi/R)] - gH(\,\mathrm{d}h/\,\mathrm{d}x) + (\tau - \tau_\mathrm{b})_x
$$
$$
+ A\nabla^2 U - \mathrm{d}(UU/H)/\,\mathrm{d}x - \mathrm{d}(UV/H)/\,\mathrm{d}y, \tag{1}
$$
$$
\mathrm{d}V/\,\mathrm{d}t = -[fU + (U\tan\phi/R)] - gH(\,\mathrm{d}h/\,\mathrm{d}y) + (\tau - \tau_\mathrm{b}) - y
$$
$$
+ A\nabla^2 V - \mathrm{d}(UV/H)/\,\mathrm{d}x - \mathrm{d}(VV/H)/\,\mathrm{d}y, \tag{2}
$$
$$
\mathrm{d}h/\,\mathrm{d}t = -[(\,\mathrm{d}U/\,\mathrm{d}x) + (1/\cos\theta)\,\mathrm{d}(V\cos\theta)/\,\mathrm{d}y] \tag{3}
$$

where $\mathbf{U} = (U, V)$ is the mass transport in the x- and y-directions; $\tau = (\tau_x, \tau_y)$, the wind stress components; $\tau_\mathrm{b} = [(\tau_\mathrm{b})_x, (\tau_\mathrm{b})_y]$, the bottom stress components; h the free surface elevation; $f = 2\Omega\sin\phi$, the Coriolis parameter; $H(x, y)$, the topography; g, the acceleration due to gravity; ∇^2, the Laplacian operator in spherical coordinates; A, the lateral friction coefficient; $\mathrm{d}x = R\cos\phi\,\mathrm{d}\phi$, the grid spacing in the longitudinal direction; and $\mathrm{d}y = R\,\mathrm{d}\theta$, the grid spacing in the latitudinal direction.

The bottom stress τ_b can be related, either linearly or nonlinearly, to the bottom velocity, which in this case has to be replaced by the averaged depth-mean velocity. For a formulation of these terms and a discussion of the typical values used in previous modelling efforts see Subsect. 2.4.1.

We finish our consideration of the model equations with a discussion of the boundary conditions. In the first set of experiments, all boundaries of the GIN Sea are closed and non-slip, so that the relevant conditions imposed on U, V and h are:

$$
U = V = 0, \quad \text{on all boundaries,} \tag{4}
$$
$$
\mathrm{d}h/\,\mathrm{d}x = (1/gH)[(\tau - \tau_\mathrm{b})_x + A(\,\mathrm{d}^2 U/\,\mathrm{d}x^2)], \quad \text{at } x = 20°\mathrm{W} - 20°\mathrm{E}, \tag{5}
$$
$$
\mathrm{d}h/\,\mathrm{d}y = (1/gH)[(\tau - \tau_\mathrm{b})_y + A(\,\mathrm{d}^2 V/\,\mathrm{d}y^2)], \quad \text{at } y = 62°\mathrm{N} - 80°\mathrm{N}. \tag{6}
$$

The vanishing of the tangential velocity implies the existence of frictional boundary layers.

2.3. NUMERICAL TECHNIQUES

The standard numerical techniques that were employed to solve the system of Eqs. (1)–(3) have been well-tested and documented in many applications and studies. A survey of finite-difference schemes for the primitive equations for a barotropic fluid has been given in [15]. Except for the treatment of the free surface, we have followed the differencing techniques applied to the barotropic component of his 3-D rigid-lid model in [16]. For a recent treatment of the free surface in shallow water simulations, the reader is referred to [17] and [18]. The formulation of a 'mesh-box Reynolds number' criterion for numerical simulation of strongly advecting flows is found in [12].

We will just give a schematic outline of the numerical techniques used. We represent Eqs. (1) and (2) in a simple format as

$$\mathrm{d}U_i/\,\mathrm{d}t = P_i + C + A(U_i) + F(U_i) + W_i, \tag{7}$$

where P_i is the pressure gradient in the i-th direction due to the surface elevation, C the Coriolis force, $A(U_i)$ the advection of the i-th component of momentum, $F(U_i)$ the lateral friction, and W_i the sum of the wind and bottom stresses in the i-th direction. Similarly, we can write Eq. (3) as

$$\mathrm{d}h/\,\mathrm{d}t = D(\mathbf{U}), \tag{8}$$

where D is the divergence of the horizontal mass transport. Upon discretizing the time coordinate as $t = n\delta t$, and denoting the value $U(t = n\delta t)$ as U^n, we can write the finite-difference schemes employed as

$$(U^{n+1} - U^{n-1})/\delta t = P^n + C^n + A^n + F^{n-1} + W^n, \tag{9}$$

$$(h^{n+1} - h^{n-1})/\delta t = D^n, \tag{10}$$

where the spatial derivatives ∇P, $U\nabla$ and ∇^2 associated with the pressure gradient, advection and friction operators are all differenced in the x- and y-directions according to standard second-order centred differences. The evaluation of all terms on the right-hand side of the equations at previous time steps, where the solution is already known, is referred to as the 'explicit method'; the new values of U at step $n + 1$ can be obtained immediately by simply summing the right-hand side. In contrast, if some of these terms had been evaluated at step $n + 1$, the method would be called an 'implicit' method, since the new values of U^n at time $t = n\delta t$ could not be obtained directly without a matrix inversion procedure; thus they are known only 'implicitly'.

Though we avoid using a matrix inverter to solve for the values at t^{n+1}, we pay the price by being restricted in the time step we can take by the speed of the surface gravity waves $c_g = gH$, such that $\delta t < \delta x/c_g$. For a maximum depth of 3500 m this gives a value of 40 s for the time-step.

Since we are interested in the steady state, the use of a time-dependent model is questionable. However, the complicated geometry and nonlinearity make an analytic solution not feasible. The inversion of the discrete-variable equations via a matrix solver seems formidable, especially since a grid of 40 × 40 points would involve inversion matrices of dimension 1600 × 1600, though they would be sparse. At any rate, nonlinearity in both the advection and bottom friction terms would tend to rule out direct inversions. Thus we are forced to arrive at the steady state by spinning-up a time-dependent model from some initial state, utilizing the proper values of bottom and lateral friction. This memorandum will discuss the establishment of these 'proper' friction values. Furthermore, the current testing of the time-dependent model with the steady winds will constitute a useful first step in the overall testing scheme of barotropic models for the GIN Sea.

2.4. BOTTOM AND LATERAL FRICTION

2.4.1. Bottom friction

Even in multi-level ocean models where an attempt is made to explicitly model the vertical structure, the effort to resolve boundary layers is usually confined to the surface mixed layers; the so-called benthic bottom boundary layer receives little attention. Generally, most ocean models resort to the application of some sort of drag law to represent the turbulent frictional processes in the lowest layer. On the other hand, the use of lateral friction is an almost universal constraint imposed on all hydrodynamic numerical models. This constraint is due to their inability to follow the cascade of energy below scales of the mesh size because of numerical stability requirements, particularly if the nonlinear terms are dominant. The bottom friction term can take either a linear or nonlinear form; both forms have been used in previous ocean models of various types.

Linear approach   This has been used by several modelers utilizing layered-type ocean models. An investigation of the energy transfers in a two layer model [6] has also derived some magnitudes for the value of σ' from spindown considerations. The recommended value of σ' is in the range 1–5×10^{-7}/s. Creegan [1] has utilized the linear drag law in a study of the wind-driven circulation in the GIN Sea, and used a value of $\sigma' = 10^{-7}$/s.

Non-linear approach   Many of the modelling efforts in the North Sea have employed a nonlinear bottom stress of the form,

$$(\tau_{\mathrm{b}})x = C_{\mathrm{d}}|U|U, \quad (\tau_{\mathrm{b}})y = C_{\mathrm{d}}|U|V \tag{11}$$

with the value of the drag coefficient C_{d} taken as either 0.0025 or 0.0050, depending on the author. Many studies [8,10,11,13,9] have used $C_{\mathrm{d}} = 0.0025$, whereas [7] and [14] have used a value of $C_{\mathrm{d}} = 0.0050$. These values were generally determined from their transient behaviour during computation of tides. In considering

an application of these values for the barotropic experiments carried out here, we must consider whether the benthic boundary layer processes in the North Sea differ significantly from the ones at the bottom of the GIN Sea. To answer this question one would need to know the typical benthic boundary layer thicknesses, interior flow speeds and the size of the turbulent eddies. On first approximation it doesn't appear that these processes would be very different at a depth of 500 m from those at, say 2500 m; hence the use of drag coefficients with the same magnitude appears to be warranted.

2.4.2. Lateral friction

The use of a lateral friction coefficient is a general requirement for modeling all hydrodynamic processes that have strong nonlinearities; as such it becomes a necessary part of ocean models as well. Such friction is necessary both for physical and numerical reasons. The size of such coefficient can be estimated from various arguments, as is the following:

The history of numerical simulation of nonlinear flows shows that the size of this friction coefficient A is determined by a constraint laid on the so-called mesh-box Reynolds number, defined as $R_c = \delta x U/A$, where δx is the mesh size and U the magnitude of the velocity in that mesh box. This number is constrained generally to take on values ≤ 4 in nonlinear flow simulations, as discussed in [12]. Though the barotropic flow modelled here behaves almost linearly, the presence of steep topography can be shown to cause effects similar to those of nonlinearity. From Eqs. (1–3) we can derive a wave equation of the form

$$\mathrm{d}h/\,\mathrm{d}t = g\nabla(H\nabla h) = gH\nabla^2 h + g\nabla H\nabla h. \tag{12}$$

The second term has the form of an advection term; in particular that $\sqrt{g\Delta H}$ represents a velocity by dimension. Inserting this velocity into the formula for the critical sub-mesh Reynolds number gives $R_c = \Delta x\sqrt{g\Delta H}/A$. Thus, if $R_c \sim \delta H$ for a bottom-slope rise of 100 m in 25 km, a value of $R_c = 4$ implies a lateral friction value of $2 \times 10^5 \mathrm{m^2/s}$; $\delta H = 1000$ m/25 km the lateral friction value is $6.10^4 \mathrm{m^2/s}$.
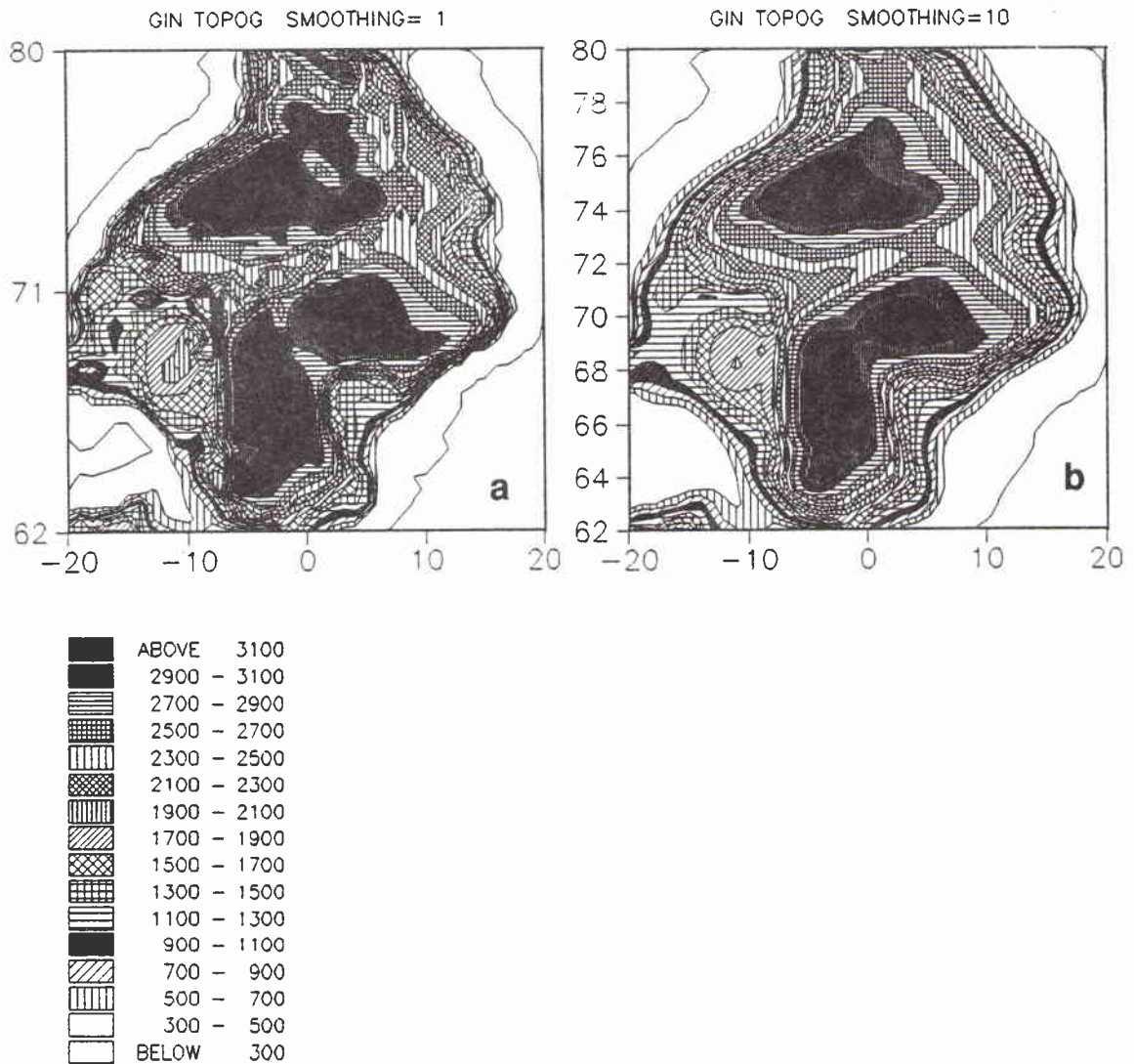
Figure 1 *GIN Sea bottom topography from a $1.0° \times 0.5°$ subgrid of the DBDB-5 topographic data set. Depths below 3100 m (black areas) form the deep sub-basins. (a) Original data; (b) smoothed version generated by 10 successive sweeps by a diffusive filter. (Depth in meters.)*

2.5. TOPOGRAPHY AND BASIN GEOMETRY

The data set chosen for generating the coastlines and the bottom topography was the digital bathymetry data base at 5-min intervals (DBDB-5) (US Naval Oceanographic Office, circa 1982). This grid is too fine for our modeling efforts, so we have utilized only the points lying on the $1° \times 0.5°$ subgrid. Later, as the model grid is refined, higher density subsets will be used.

Figure 1 illustrates the topography on the $1° \times 0.5°$ subgrid. Figure 1a shows the topography before any smoothings are introduced. Figure 1b shows a smoothed

version obtained with ten successive sweeps by a diffusive filter. The smoothing slightly modifies the shapes of the deep basins (dark black areas), some local shallow areas around $75°N, 2°E$ and $65°N, 6°W$, a local high around $68°N, 11°W$, and also causes the disappearance of the individual seamounts along the Jan Mayen Ridge (e.g. $69°N, 8°W$). As we shall see in Sect. 3, however, even this smooth topography will lead to some very complicated solutions and some numerical problems for the barotropic solution.

2.6. FORCING

The circulation in a barotropic ocean is generally the result of two kinds of forcings; the wind stress at the ocean's surface, and the source–sink mass flows at the basin boundaries. The source flows could be ocean currents that enter the GIN basin due to wind-forcing in an adjacent basin, or to replace water mass driven out by the wind or baroclinic pressure gradients in the GIN basin. Sink flows have similar origins. However, in this first paper on the barotropic circulation we will only consider closed boundaries, and confine ourselves to a discussion of the wind forcing.

During the model testing stage, we will utilize only steady winds. With constant wind-forcing the ocean will generally arrive at a steady circulation via a spin-up process. Steady winds are also customarily used in theoretical studies to study the balance of forces and energy conversions, and to obtain the mean or climatological circulation.

Climatological wind fields in the past have usually been computed from many years of ship observations. However they are also obtained from a series of analyzed pressure or wind field outputs of weather prediction models. Aagaard [3] computed the annual and monthly mean wind stresses for the year 1965 from the Norwegian Meteorological Office's analyzed pressure charts for that year. In this memorandum the monthly-averaged wind stresses will be obtained from the output of a Planetary Boundary Layer Model at the Fleet Numerical Oceanography Center (Monterey, CA) for the years 1985, 1987 and 1988.

2.6.1. Monthly mean winds

We have taken the mean winds for July, September and the annual mean wind for 1965 as they appear in Figs. 1–3 of Aagaard [3]. The stresses are given in tenths of dynes over an area $20°W–20°E$ and $64°N–78°N$, on a grid of $5° \times 2°$ squares. We have interpolated them onto a grid of $1.25° \times 0.5°$ squares using cubic splines. Altogether 41 data points are given on a 9×8 grid, implying that 31 (i.e. $72 - 41$) data points are missing. Our first attempt to fill in the missing values by a direct application of the bi-cubic spline routines of the NAG library left us with an unsatisfactory curl of the stress field. Therefore we resorted to subjective analysis, particularly near

the edges of the basin where extrapolation, rather than interpolation was required. During this analysis the following three factors were considered:

(a) Only the land points near the ocean/land boundaries were utilized.

(b) The nature of the curl ($d\tau_y/dx - d\tau_x/dy$) suggests that along constant latitude lines τ_y should be weighted more heavily, and along constant longitude lines τ_x should be weighted more heavily.

(c) Extrapolation to replace the missing values near the boundary region was extended only to two points lying outside the last known data point; only single points were needed for interpolation.

2.6.2. General Circulation Model (GCM 1985 and 1987/8) winds from FNOC

The GIN Sea area obviously lacks a network of airport towers and radiosonde locations to report weather observations; nor is it the area of preferred shipping lanes. Therefore, the weather data is relatively sparse and doesn't favour analysis and accurate prediction. We can expect that, at least daily, the surface stress fields, obtainable only from special sources, may be inaccurate. One of these sources is the output of General Circulation Models (GCM) for prediction.

The US Navy at Fleet Numerical Oceanography Center (FNOC) also operates a daily General Circulation Model covering the world; its output is available every 6 h in near-real time. One can obtain two sets of winds, computed by different models at two different height levels. One, at the 10 m level above the surface, is computed by the Planetary Boundary Layer Model (PBLM), using output fields of the Global Weather Prediction Model (GWPM). Winds at the 50 m level are direct outputs of the GWPM. The surface heat flux components are all outputs of the PBL.

FNOC has provided two sets of GCM fluxes which cover the periods February–August 1985 and 14 April 1987–15 May 1988. Both sets represent synoptic fields from the GWPM at 6 h intervals. Each set contains six fields: surface pressure, solar radiation, total surface heat flux, east–west marine wind, north–south marine wind, and total surface moisture flux. The wind fields were deficient because they were processed through a boundary layer model which is primarily concerned with local and mesoscale processes, and generally ignores the preservation of the large-scale wind curls associated with the global winds that drive the PBLM. Yet these wind curls are very important to driving the ocean circulation.

The European Centre for Medium-Range Weather Forecasting (ECMWF) has another data base. The ECMWF fluxes are available from 1 July 1985 but, though requested, were not available in time for this memorandum.

Significant seasonal and year-to-year variations in the intensity and spatial distribution of the wind curl also occur over the GIN Sea. As seen below, the curls in

the spring of 1985 exhibit great coherence over the whole GIN Sea during the entire spring season, whereas the 1987 winds for the corresponding period show irregular curl patterns.

The fluxes come on the original spherical grid of $2.5° \times 2.5°$ resolution. We have used the subset for the European window ($25°W$–$35°E$, $30°N$–$80°N$) to extract a further subset over the GIN Sea ($20°W$–$20°E$ and $62.5°N$–$80°N$). The last subset represents a mesh of 21×9 grid points. These were interpolated onto a 41×36 mesh via cubic splines to give a $1° \times 0.5°$ resolution in the east–west and north–south directions, respectively.

The GCM presents the wind velocities at 19.5 m above the surface. These velocities must be converted to stresses at the surface by multiplying them by 0.943. This brings the winds down to the 10 m height, where the standard stress formula can be applied, thus

$$\tau_i = \rho_a C_d |U| U_i \tag{13}$$

where ρ_a is the air density ($= 1.25$ kg/m^3) and C_d is the drag coefficient taken as

$$C_d = (0.90 + 0.06|U|)10^{-3}. \tag{14}$$

The values of the constants appearing in Eq. (14) have been taken from [19], and agree very closely with the values used in [20].

3

Model testing

The initial testing of numerical ocean models is usually performed under simplified conditions, using steady winds, closed ports, constant friction coefficients, and even flat bottoms or strongly smoothed topography. Later, specific tests are designed to study the behaviour of the models with the inclusion of previously omitted complexities, usually one at a time. These more specific tests are necessary because ultimately the success of ocean models depends more on simulating faithfully the observed oceanographic phenomena than on satisfying certain numerical and physical constraints, necessary conditions but not sufficient. For example, a model can conserve mass and energy very accurately and still be swamped by small-scale noise, causing mislocation and under- or overestimating the strength of an eddy.
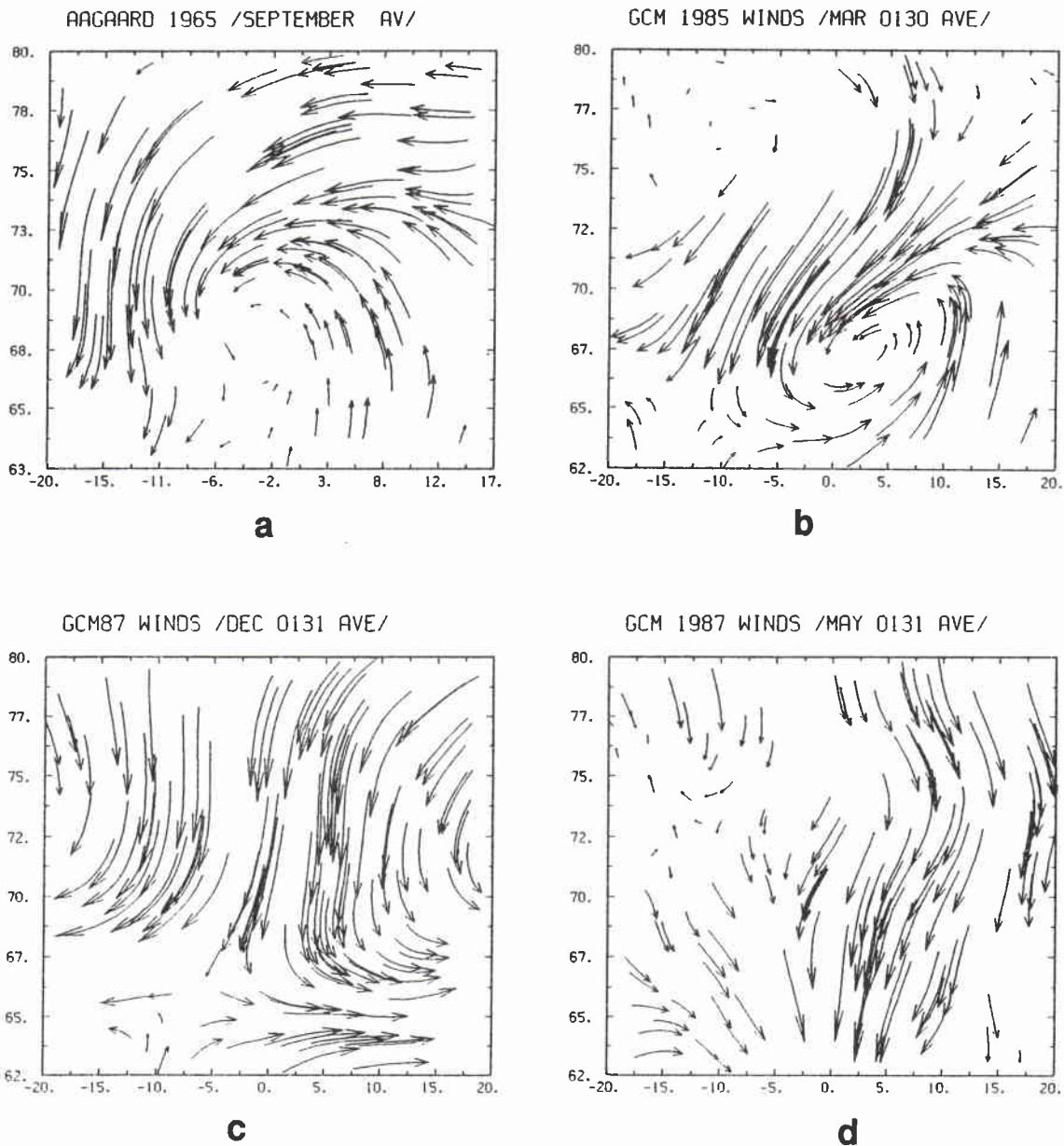
We have tested our barotropic model systematically. First we tested the numerical scheme for conservation of mass and energy, and then separately examined the dependence of the computed flow on bottom and lateral friction, on the smoothing of the topography, and on the time-dependence of the atmospheric forcing. The conservation tests were carried out without forcing, using a large-amplitude oscillating seiche as the test medium. These results are presented in Subsect. 3.1. The effects of friction and topography in the presence of steady winds are presented in Subsect. 3.1.2. The results of the time-dependent studies will be presented in a subsequent report.

To examine the frictional effects, we tried both the linear and nonlinear bottom friction formulations. Also, we used a range of values for the lateral friction coefficient A spanning four orders of magnitude ($A = 10$ to 10^4 m^2/s). The bottom friction tests were carried out for only one set of wind forcing [case (i), see below]. The search for an optimum, or at least adequate, value of the lateral friction coefficient was carried out for several sets of wind fields [cases (i)—(iv)], since the diffusion operator associated with A dampens the shorter spatial scales much more strongly.

To examine the effects of topography and its numerical treatment, we have run identical cases for flat, rough and smoothed topography. The smoothed topography is generated by successive applications of a diffusive filter to the full-depth topography. The various degrees of smoothings were tested with only the wind fields of case (i); for all other applications of the topography factor ten applications of the diffusive filter was used to smooth.

In particular, we have investigated the dynamic effects of diverse spatial scales in

AAGAARD 1965 /SEPTEMBER AV/

GCM 1985 WINDS /MAR 0130 AVE/

a

b

GCM87 WINDS /DEC 0131 AVE/

GCM 1987 WINDS /MAY 0131 AVE/

c

d

Figure 2 *Averaged wind stress fields, based on associated curl patterns, in order of increasing irregularity and small-scale content (see Fig. 3): (a) September 1965; (b) March 1985; (c) December 1987; and (d) May 1987.*

wind forcing. The most important property of the winds forcing an ocean is the curl of the wind stress, since this is translated into a corresponding vorticity pattern, and thus, into oceanic circulation. We wanted to find out if the diverse forcing scales lead to corresponding scale selections in the ocean circulation. We have performed tests with four classes of steady wind fields, for which the stress vectors and corresponding curl patterns (see Figs. 2 and 3) were arranged in order of decreasing coherence and increasing short wavelength content. These classes are described as follows:
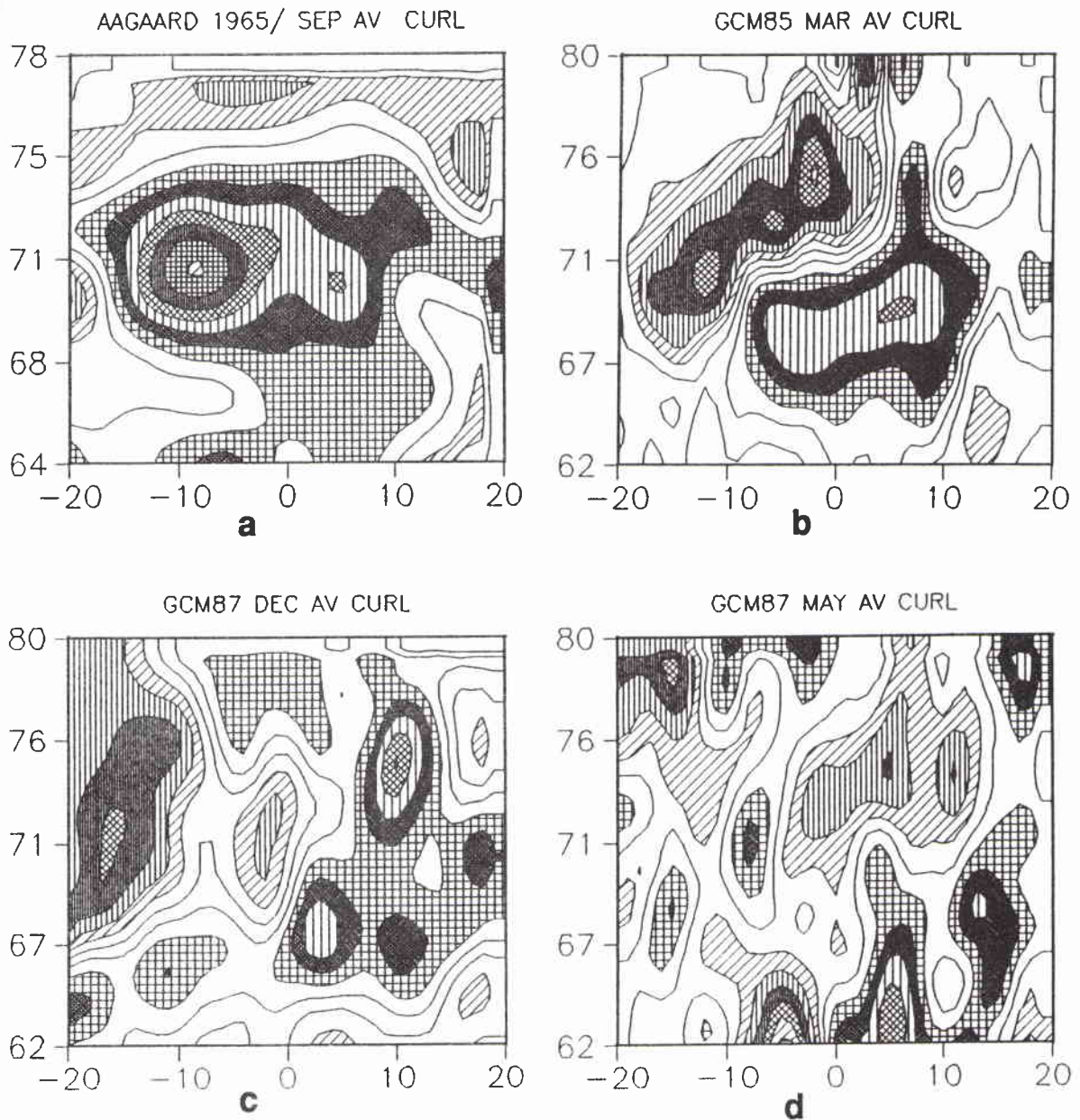
Figure 3 *Respective curl field intensities in the averaged wind stress fields illustrated in Fig. 2 (see Fig. 4 for intensity scales). Only the short-wavelength patterns are shown. (a) September 1965, (b) March 1985, (c) December 1987, and (d) May 1987.*

(i) A wind field having a monotonic curl over the whole GIN Sea basin (Figs. 2 and 4a). In this case we have chosen the September '65 average winds [from Aagaard (1970)], showing a strong low pressure cyclone centered about 71°N, 10°W.

(ii) A wind field having a curl with scales of the order of half the basin size

(Figs. 2b and 4b). In this case we have chosen the March 1985 average winds, showing a high pressure anti-cyclone in the north–west quadrant of the GIN Sea (probably related to the Greenland High), and a low-pressure cyclone in the southeastern quadrant, centered over the Norwegian Sea at 69°N, 8°W.

(iii) A wind field having a curl with spatial scales of the order of a quarter or less of the basin size (Figs. 2c and 5a). Here we have chosen the December '87 average winds, which show two high pressure anti-cyclones (negative curl) loosely connected and centered at 71°N, 17°W and 71°N, 2°W, respectively, and several low pressure cyclones, of which the two strongest ones are centered at 74°N, 10°E and 67°N, 2°E, respectively.

(iv) Finally, a wind field consisting of an irregular distribution of small-scale pressure centers, both cyclonic and anti-cyclonic (Figs. 2d and 5b). In this case we have chosen the May 1987 average winds.

Figures 2 and 3 indicate that the relation between the stress vector patterns and their curl fields is subtle. Certainly, the December '87 winds in the northern two-thirds of Fig. 2c and the May '87 winds in the eastern half of Fig. 2d appear smooth. Qualitatively they are no different from the September '65 (Fig. 2a) and March '85 (Fig. 2b) winds, yet their associated curl fields are much more complex. A partial explanation can be found in the fact that the wind stress vectors of Fig. 2 also include the divergent wind component, which is automatically eliminated upon taking the curl.

3.1. CONSERVATION OF MASS AND ENERGY

3.1.1. Steady winds and spinup

The second test to be performed on the barotropic model was forcing by a steady wind. Unlike the test with seiches where no energy has been imparted to the system, a power input proportional to $\overline{U\tau}$ is deposited into the ocean. In order that the energy and mass conservation may be more thoroughly tested, no in- or outflow through the boundaries is allowed. A steady wind forcing the ocean will generally produce a steady circulation. For a medium-size grid which does not resolve small barotropic instabilities or eddies, and for sufficiently large values of the bottom and lateral friction, the circulation evolves directly to the final state in a monotonic manner, without substantial changes in the local patterns. This approach to a steady circulation is called the 'spinup' process.

We must also consider the spatial scales of the winds as well as their time-scales. As discussed above, we performed tests with different classes of winds, based on the scales of their associated curls.
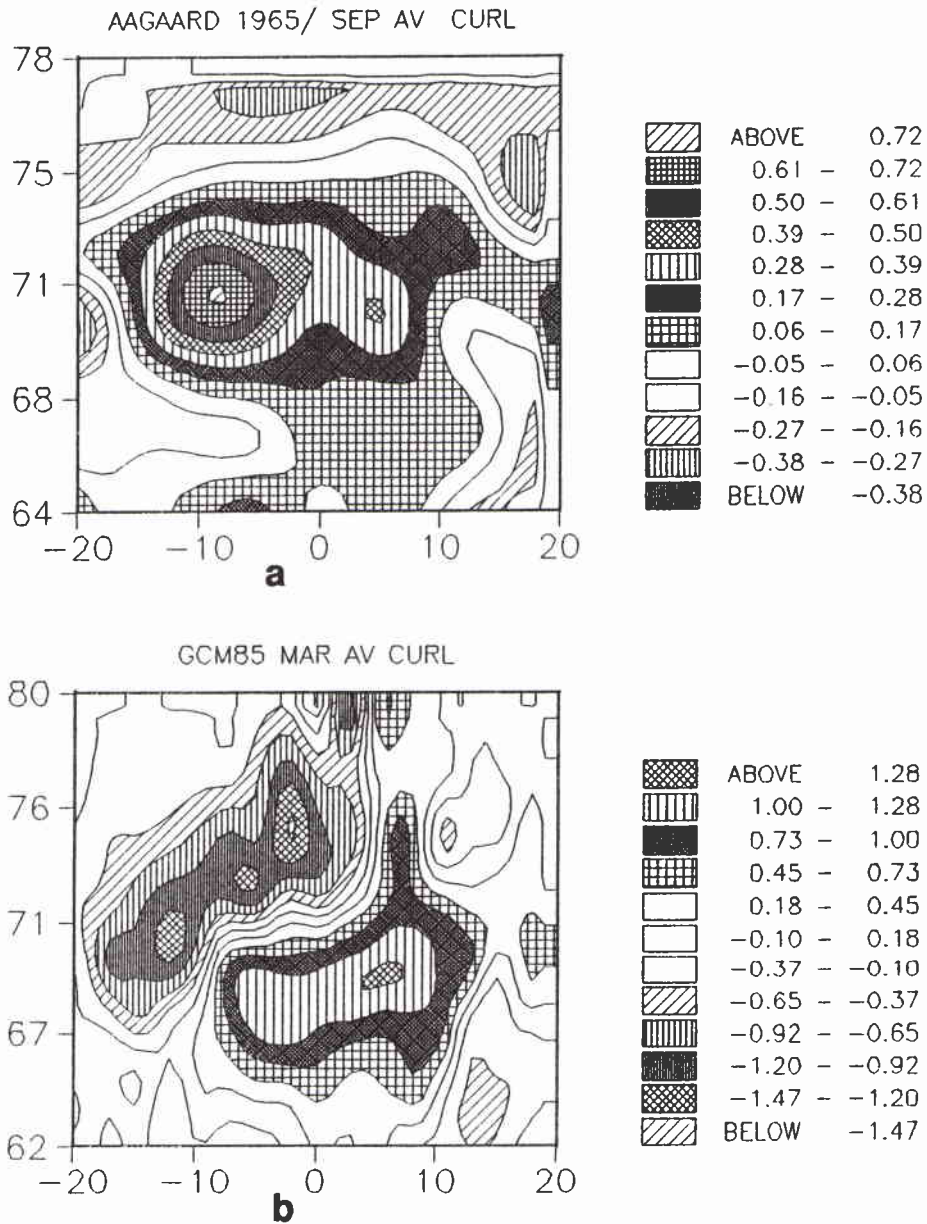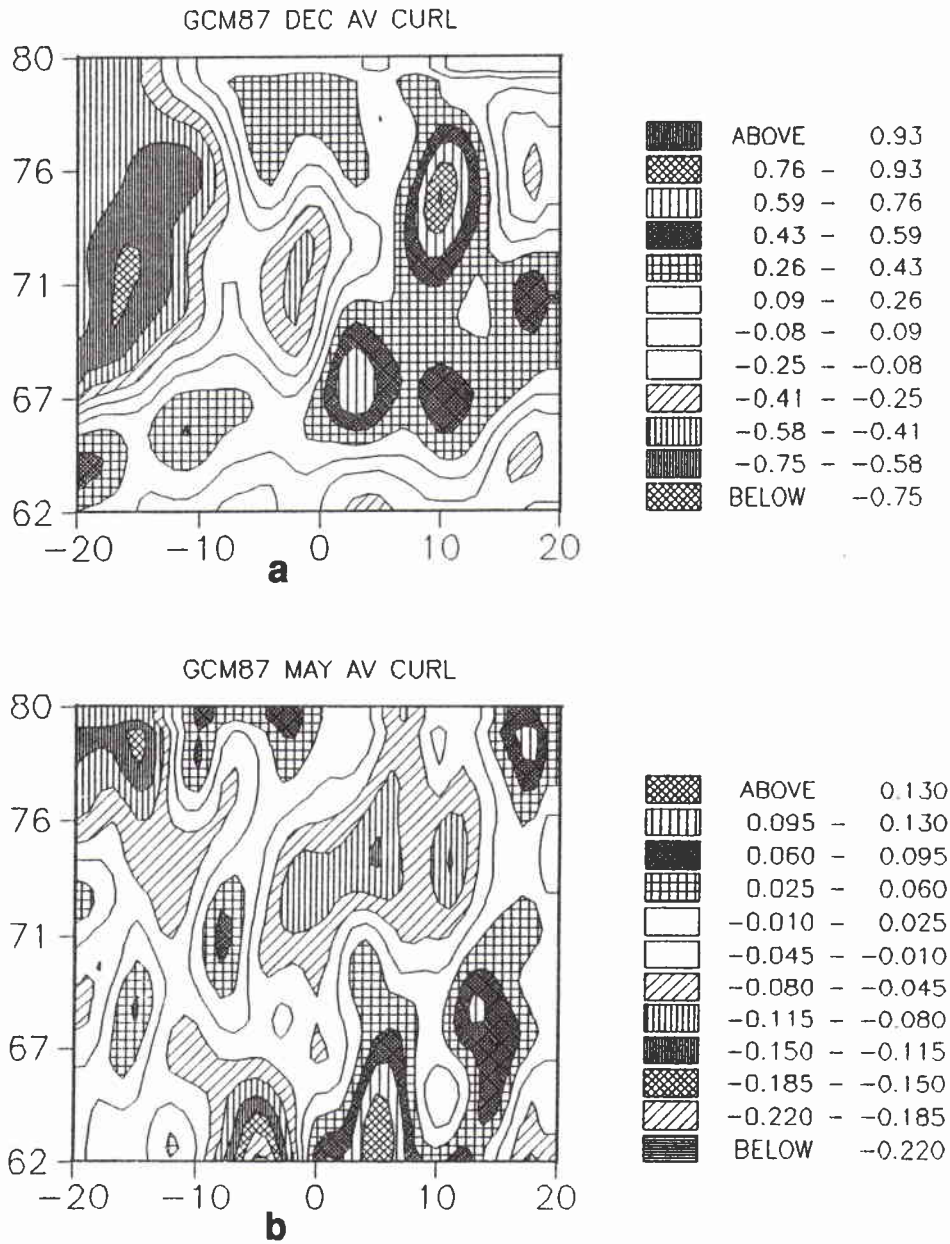
Figure 4 *Intensity contours and associated scales for the (a) September 1965, and (b) March 1985 wind curls shown in Fig. 3. (Curl units are 10^{-6} m/s.)*

3.1.2. Winds with monotonic basin-scale curl: September '65

Figure 4 presents intensity contours and the associated scales for the September '65 and March '85 wind curls shown in Fig. 3; Figure 5 presents the same information for the wind curls of December '87 (a) and May '87 (b).

The average winds for September '65 (Fig. 4a) exhibit the extreme monotonicity of

Figure 5 *Intensity contours and associated scales for the (a) December 1987, and (b) May 1987 wind curls shown in Fig. 3. (Curl units are 10^{-6} m/s.)*

the curl over the GIN Sea. A strong cyclonic vortex, covering almost the whole basin, produces a clockwise circulation with peak winds up to 1.8 dynes/cm^2. Figure 6 is presented to allow the direct comparison of the wind vectors and the curl contours; though it appears uninteresting for this case, such a comparison for other periods becomes very instructive. The areas below 64°N and above 78°N were extrapolated, and probably show anomalously large, possibly false, negative values of the curl (anti-cyclonic motion).

SACLANTCEN SM-242
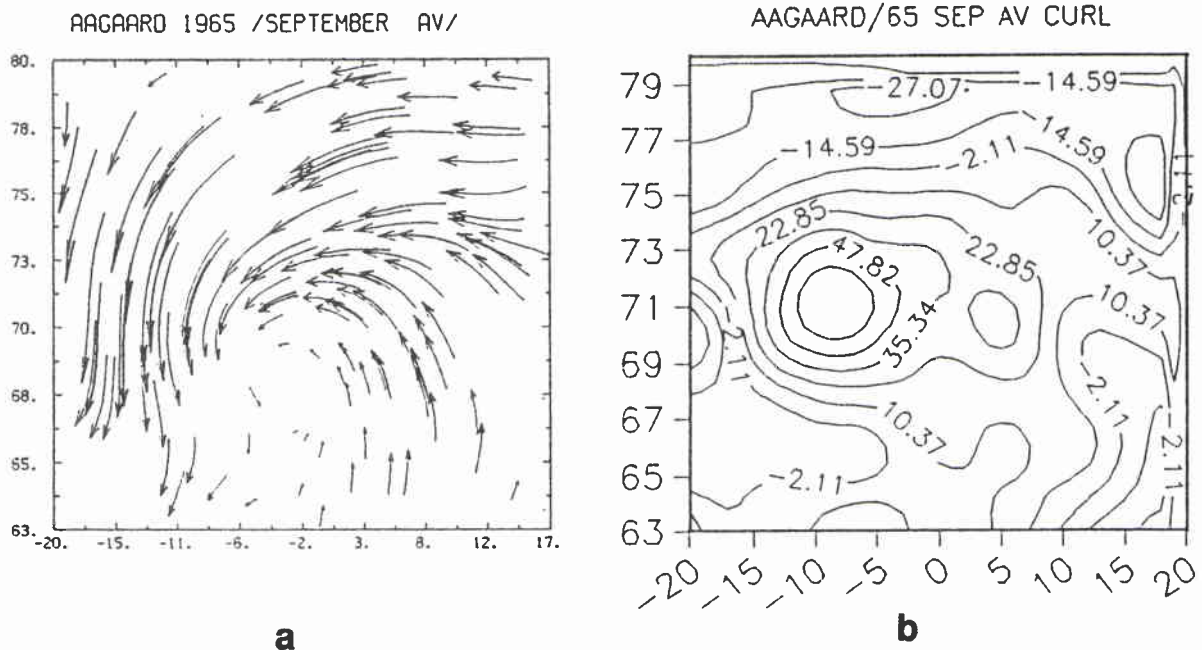
Figure 6 *The September 1965 average (a) wind stress, and (b) its curl field, based on Aagaard's [1970] computations from pressure fields supplied by the Norwegian Meteorological Office. (Curl units are 10^{-6} m/s.)*
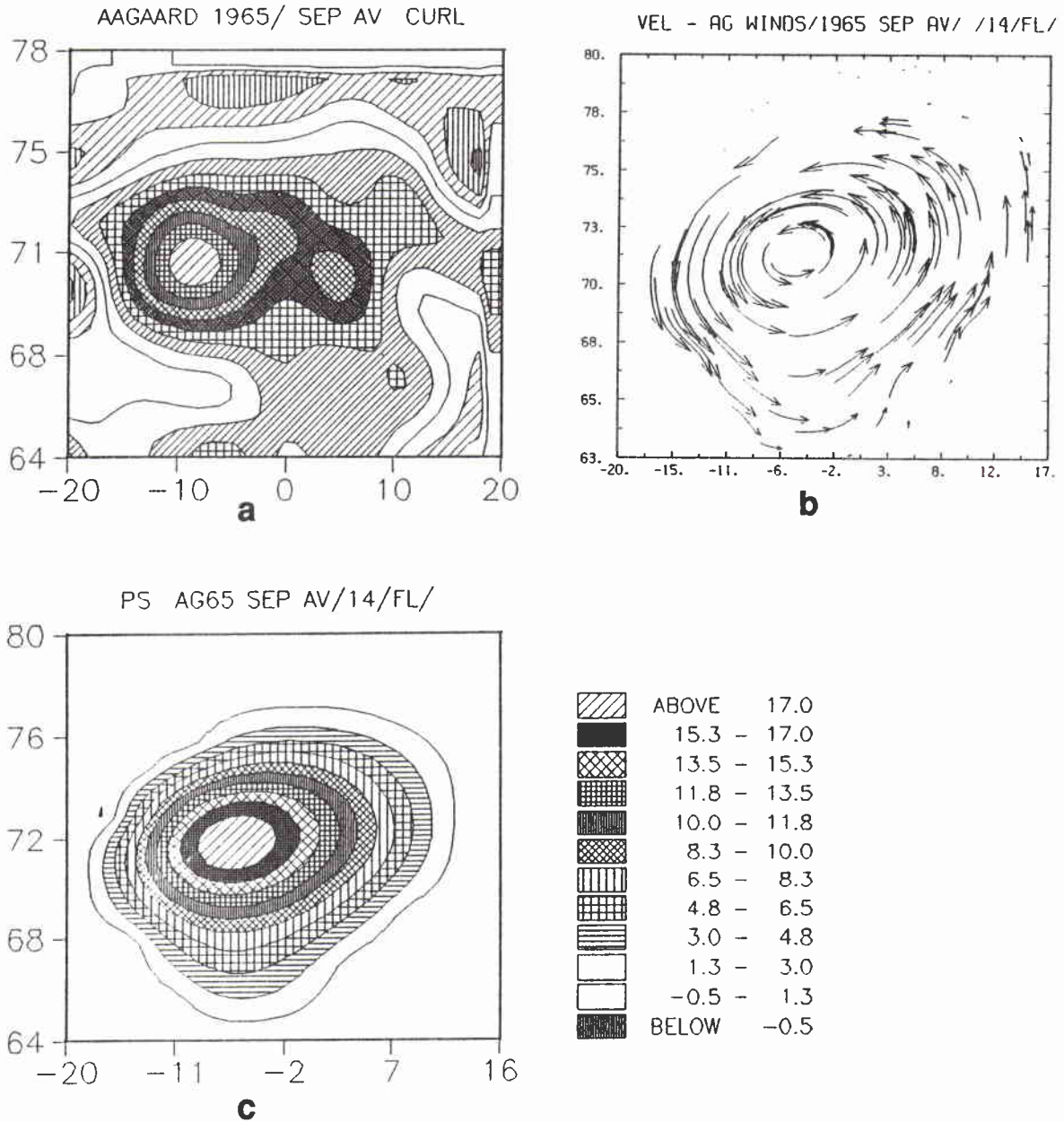
Flat bottom case The wind curl contours, mass transport vectors and corresponding streamline contours for $A = 10$ m^2/s are shown in Fig. 7. The ocean circulation consists of a large cyclonic gyre enveloping most of the GIN Sea, as expected, in response to the large atmospheric cyclone dominating the whole region. The only significant deviations from symmetry appear to be a northward jet along the boundary adjacent to the Barents Sea, and a southward extension of the gyre just north of the Faeroe Islands. Since the atmospheric vortex itself is not perfectly symmetric, deviations from symmetry are also expected in the oceanic circulation. A small cyclonic vortex (70°N,5°E), attached to the eastern end of the main atmospheric vortex, along with a general southward extension of some low level positive wind curl, could be the driving force behind the southward deflection of the otherwise symmetric oceanic gyre.

On the other hand, the northward jet adjacent to the Barents Sea has causes other than the asymmetry of the atmospheric vortex. This asymmetry is present with various degrees of intensity in all the wind-forcing cases examined in this study.

The mass transport streamlines and the surface elevation contours are shown in Fig. 8 for two values of the lateral friction coefficient $A = 10^4$ m^2/s (top row) and $A = 10$ cm^2/s (bottom row), respectively. For $A = 10$ the solution needed 40 days to converge, and for $A = 10^4$ only 20. Apparently the lateral friction coefficient has almost no visible effect on the circulation patterns, even over four orders of magnitude ($A = 10$ to 10^4 cm/s). Neither the transport vectors nor the streamlines show any effects; only the intensity of the circulation does. As expected,

AAGAARD 1965/ SEP AV CURL

VEL - AG WINDS/1965 SEP AV/ /14/FL/

PS AG65 SEP AV/14/FL/

|	
ABOVE	17.0
15.3 −	17.0
13.5 −	15.3
11.8 −	13.5
10.0 −	11.8
8.3 −	10.0
6.5 −	8.3
4.8 −	6.5
3.0 −	4.8
1.3 −	3.0
−0.5 −	1.3
BELOW	−0.5

Figure 7 *The circulation forced by the September 1965 monthly mean wind stress in a flat bottom GIN Sea basin: (a) wind curl, (b) mass transport vectors, and (c) mass transport streamlines. (Curl units are 10^{-6} m/s; streamline units are 10^{6} m³/s.)*

the strongest circulation occurs for the lowest value of $A(=10$ m/s). Even for $A = 10$ m²/s the circulation patterns appear smooth and stable. This implies that, at least for the flat bottom case, one can employ very low values of the lateral friction coefficient without encountering the numerical difficulties anticipated and described in Subsect. 2.4.2.
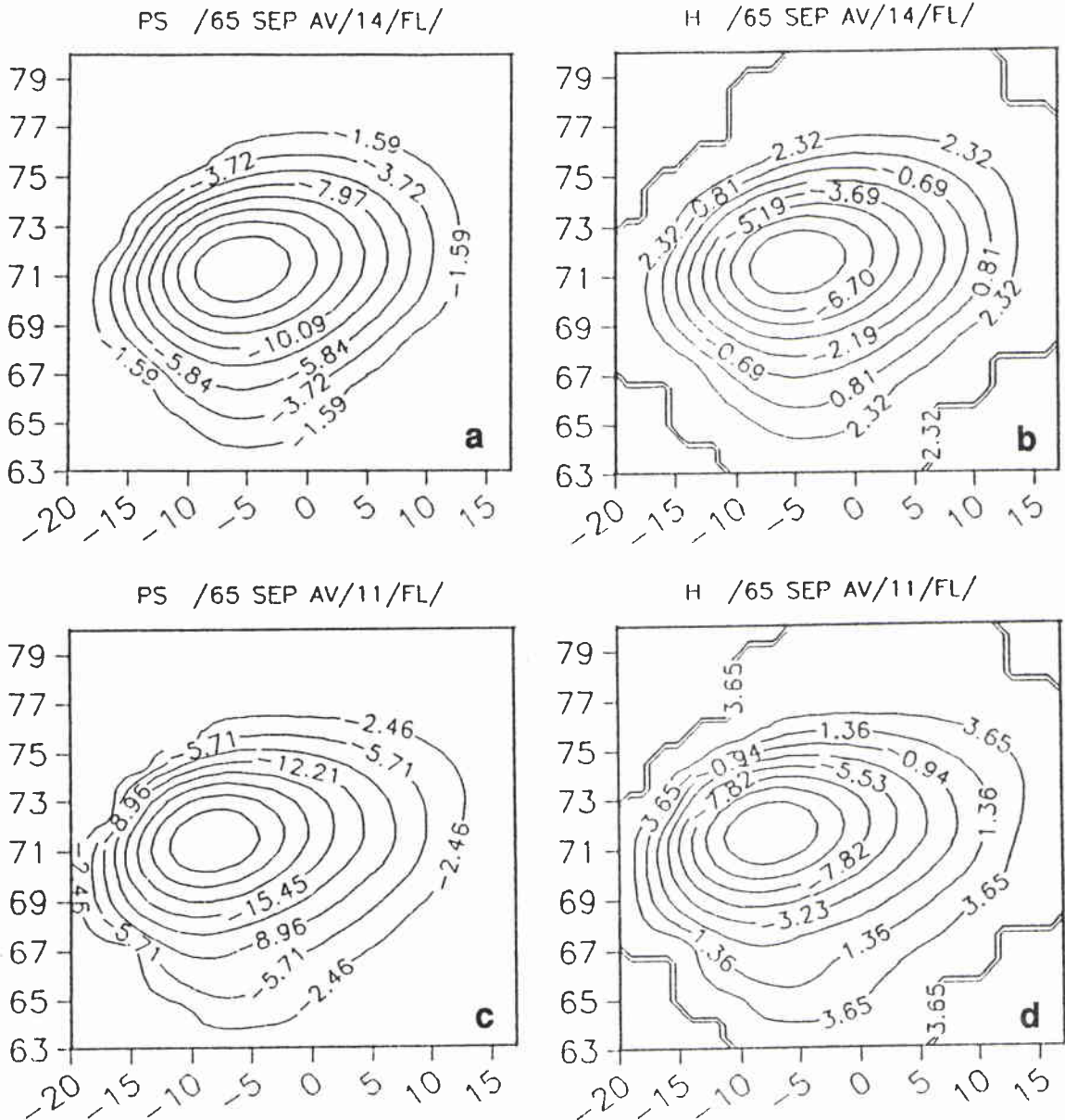
Figure 8 *The influence of horizontal friction on the September 1965 circulation in a flat-bottom GIN Sea basin: (a) streamlines, (b) surface elevation for 10^4 m^2/s, (c) streamlines, and (d) surface elevation for $A = 10$ m^2/s. (Streamline units are 10^6 m^3/s; surface elevations is in cm.)*

An examination of the streamlines and surface heights in Fig. 8 also shows that the contour lines of Ψ and h are parallel and the patterns coincide closely. A similar conclusion can be reached for simulations with the other fields, in the presence of a flat bottom. This is explained in the following paragraph.

We assume a steady state, and neglect friction and the nonlinear terms which are negligible for the deep barotropic circulation. Then taking the curl of Eqs. (1) and (2), we can derive a relation for the vorticity $\zeta = (V_x - U_y)$ thus

$$\zeta = (1/f)(gH\nabla^2 h - \beta U), \tag{15}$$

whereas from the relation of vorticity and stream function we have

$$\zeta = \nabla^2 \Psi. \tag{16}$$

A close coincidence between the isolines of Ψ and h is implied by the above relations provided the term βU is small. A comparison of the magnitudes of βU and $gH\nabla^2 h$ reveals that βU is $1/5$ to $1/10$ smaller over most of the GIN Sea domain, particularly since β decreases as the $\cos^2$ of the latitude θ. Therefore $h \sim \Psi$ and the isolines will tend to coincide.

Tables 1 and 2 display the maximum/minimum values of the surface height elevation h and the mass transport stream function Ψ, respectively, as a function of the lateral friction coefficient A. The amplitudes of the surface elevation in general depend on the value of A, the topography and the wind stress. For the September '65 circulation, with a flat bottom, the magnitudes of the surface elevation $|h|$ range from 9.70–14.7 cm for A in the range $10^4 - 10$ m^2/s, respectively (Table 1). The difference between the cases for $A = 10$ and $A = 10^2$ is negligible, but for $A = 10^3$ it is reduced about 22% and for $A = 10^4$ by 34%. The amplitudes of the mass transport stream function $|\Psi|$ for the flat bottom simulations (Table 2) range from $(18.6 - 28.4) \times 10^6$ m^3/s, for the friction range $10^4 - 10$ m^2/s. Essentially no differences appear between the results for $A = 10$ and $A = 10^2$; however, for $A = 10^3$ and 10^4 m^2/s the amplitudes are again reduced about 20% and 34%, respectively.

If the strength of the simulated circulation is considered, frictional coefficient values such as $A = 10^4$ may not be acceptable. However, if other reasons compel us to use such values, as in the topographic case (see below), we must scale the magnitudes of the computed currents and surface elevation amplitudes according to the results presented in Tables 1 and 2.

The GIN Sea topography case   The wind vectors, current vectors and mass transport streamline patterns corresponding to the GIN Sea topography simulations with $A = 10^4$ m^2/s are shown in Fig. 9. The effects of topography on these fields are immediately apparent. The current vectors and streamlines follow closely the topography contours in most of the basin. Though the general direction of the circulation set-up (in this case, cyclonic) still depends on the wind forcing; both the exact boundary of the oceanic gyre and the strength of the circulation are strongly influenced by the topography. Figure 9 further illustrates the effect of topography: the streamline contours closely parallel the topographic contours. In fact, three sub-gyres nestled more or less within the three deep sub-basins of the GIN Sea are superimposed upon the large single gyre of the flat bottom case.

Table 1 *Surface height (h) maxima/minima as a function of friction and season in the GIN Sea*

A (m²/s) = 10	10²	10³	10⁴
FB/GT*	FB/GT	FB/GT	FB/GT
September 1965 (Aagaard)			
h_{max} (cm) 3.8/0.85	4.8/2.3	5.9/2.3	5.9/2.3
h_{min} (cm) $-9.7/-0.90$	$-11.4/-1.4$	$-14.7/-1.5$	$-14.7/-1.6$
March 1985 (GCM-FNOC)			
h_{max} (cm) 10.0/4.2	18.0/6.2	19.0/6.8	20.0/7.1
h_{min} (cm) $-18.0/-5.4$	$-27.0/-8.0$	$-29.0/-8.4$	$-28.0/-8.6$
December 1987 (GCM-FNOC)			
h_{max} (cm) 5.0/1.3	8.3/2.1	9.2/2.2	9.2/2.5
h_{min} (cm) $-4.6/-0.9$	$-6.4/-1.6$	$-6.7/-1.7$	$-6.6/-1.8$

* FB – flat bottom; GT – GIN Sea topography

Table 2 *Mass transport stream function (Ψ) maxima/minima as a function of friction and season*

A (m²/s) = 10	10²	10³	10⁴
FB/GT*	FB/GT	FB/GT	FB/GT
September 1965 (Aagaard)			
Ψ_{max} (10^6 m³/s) 0.53/0.13	0.67/0.40	0.78/0.46	0.78/0.53
Ψ_{min} (10^6 m³/s) $-18.6/-2.6$	$-22.5/-3.9$	$-28.3/-4.5$	$-28.4/-4.70$
March 1985 (GCM-FNOC)			
Ψ_{max} (10^6 m³/s) 16.0/11.0	27.0/16.0	28.0/18.0	29.0/19.0
Ψ_{min} (10^6 m³/s) $-35.0/-13.0$	$-54.0/-21.0$	$-57.0/-22.0$	$-56.0/-23.0$
December 1987 (GCM-FNOC)			
Ψ_{max} (10^6 m³/s) 4.3/0.8	6.0/1.7	6.5/2.2	6.5/2.4
Ψ_{min} (10^6 m³/s) $-7.9/-2.1$	$-13.0/-4.2$	$-14.0/-4.6$	$-14.1/-4.8$

* FB – flat bottom; GT – GIN Sea topography
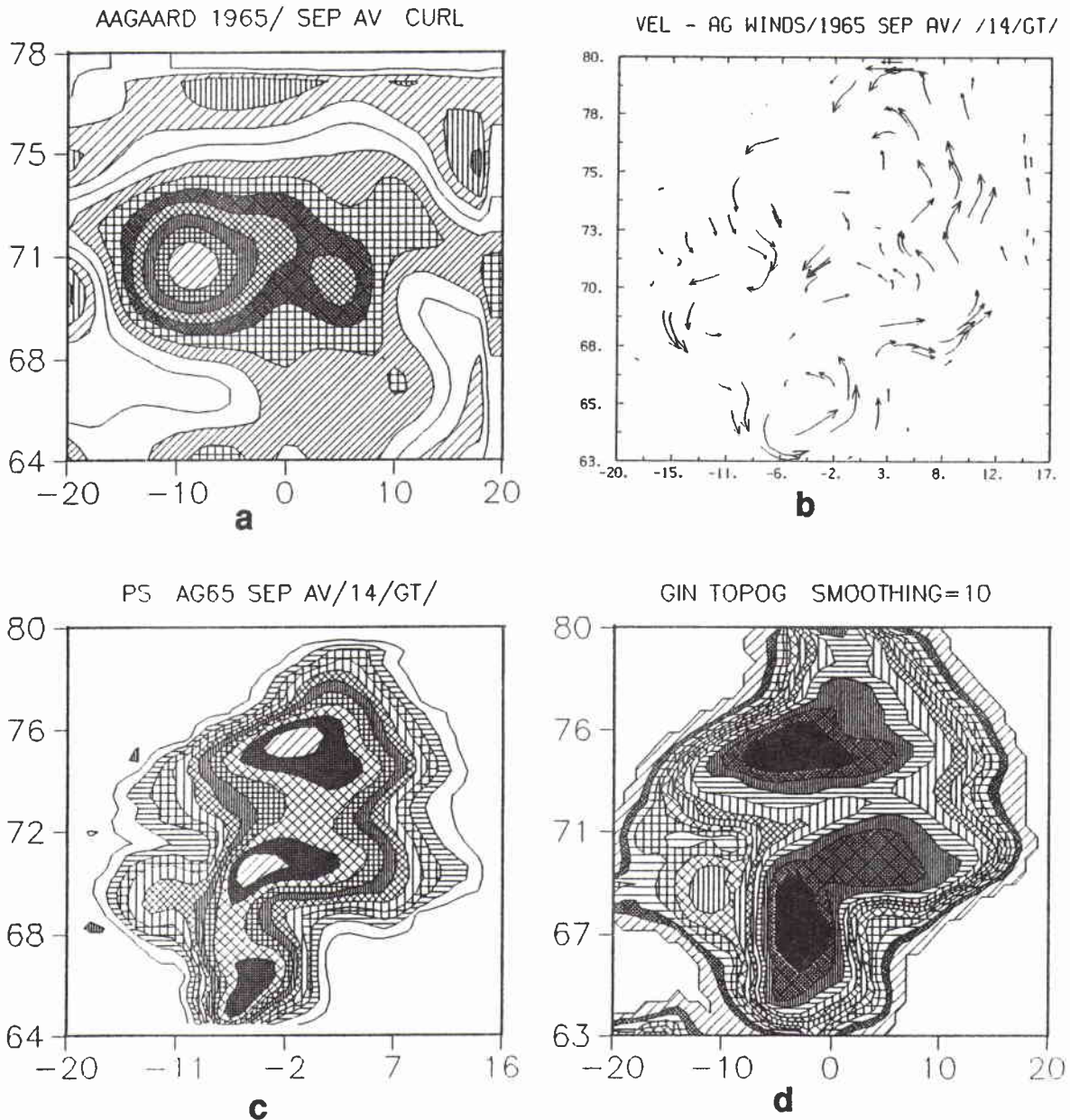
Figure 9 *The circulation forced by the September 1965 monthly mean wind stress, using the GIN Sea topography given in Fig. 1b and the lateral friction coefficient, $A = 10\ m^2/s$: (a) wind curl, (b) mass transport vectors, (c) mass transport streamlines, and (d) topography (see Fig. 1 for scale). (Curl units are $10^{-6}\ m/s$; streamline units are $10^6\ m^3/s$.)*

As in the flat bottom simulations, we have investigated the effect of the lateral friction coefficient A upon the circulation. The results are presented in Fig. 10. Figures 10a and b contain the mass transport vectors, streamlines and surface elevation for $A = 10^4$; Figs. 10c and d contain the corresponding fields for $A = 10$. The solutions converged in 20 days for the first and in 60 days for the second case.
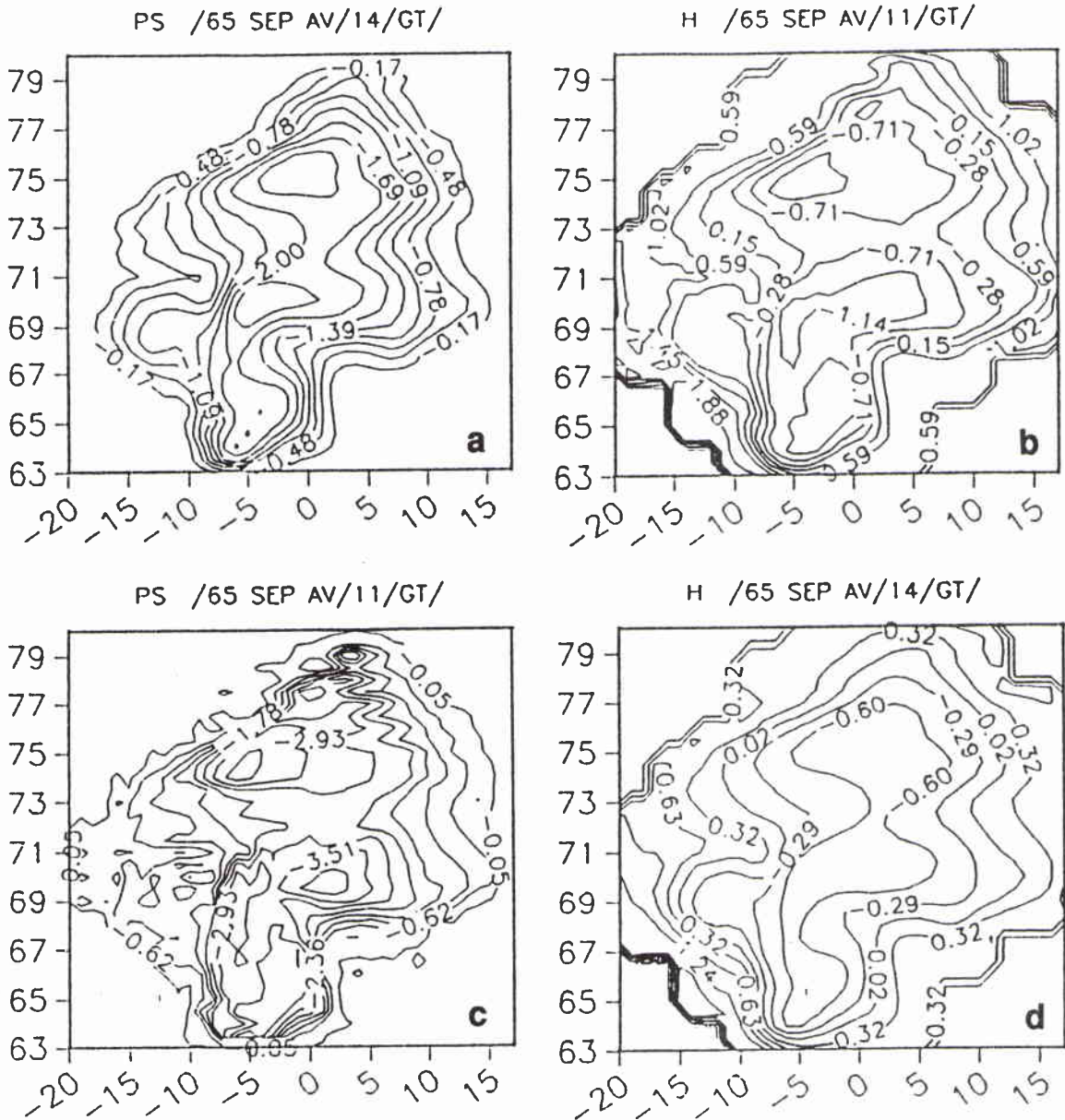
Figure 10 *The effect of horizontal friction on the September 1965 circulation in a GIN basin with smoothed topography: (a) mass transport vectors, (b) mass transport streamlines and surface elevation for $A = 10^4$ m^2/s; (c) mass transport vectors, and (d) mass transport streamlines and surface elevations for $A = 10^2$ m^2/s. (Streamline units are 10^6 m^3/s; sea surface elevations in cm.)*

For $A = 10^4$ the solutions look smooth like in the flat bottom simulations, but for $A = 10$ the stream function plots contain an unacceptable amount of noise. The height field tends to remain smooth even for those values of the lateral friction, indicating that the interaction of the vorticity field with the topography does indeed
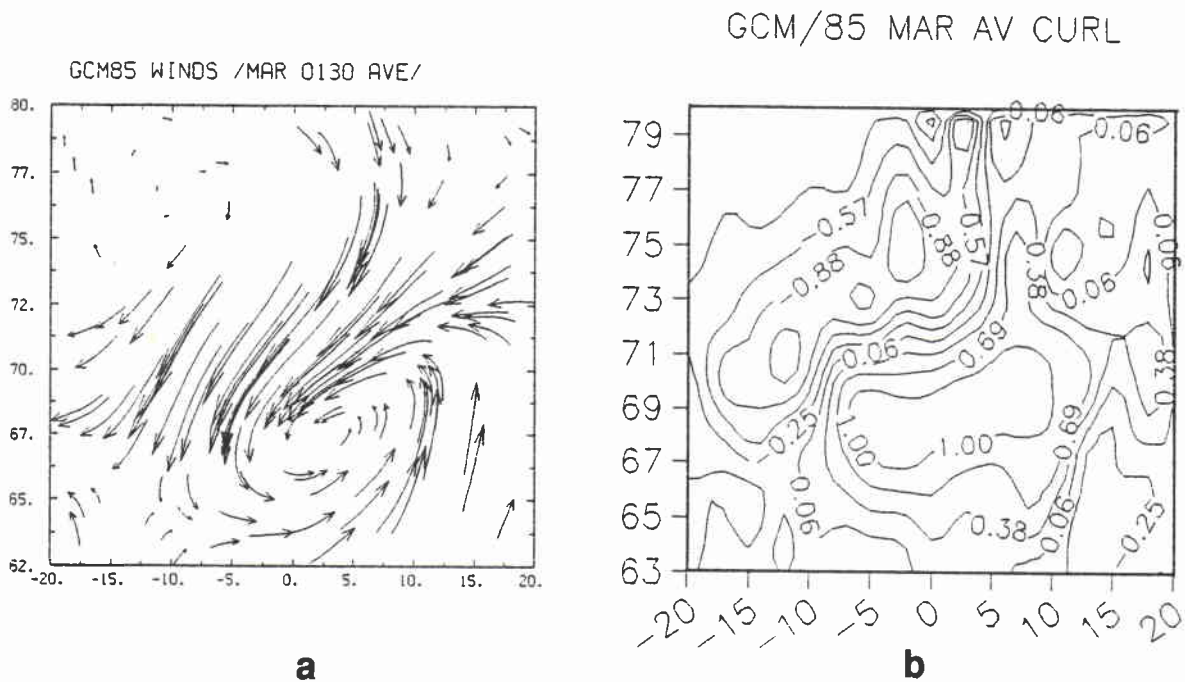
Figure 11 *The March 1985 (a) average wind stress field, and (b) its curl. (Curl units are 10^{-6} m/s.)*

introduce noise into the system.

The percentage drops of the mass transport stream function $|\Psi|$ maxima (see Table 2), corresponding to $A = 10^4, 10^3$ and 10^2, are 0.04%, 18% and 45%, respectively, based on the value for $A = 10$. We can thus perform simulations easily with lateral friction values up to 10^2 m^2/s or so, before the actual magnitude of the solutions is appreciably reduced. However, the noise content of the solution constrains us to use values above 10^3 m^2/s, and to resort to scaling to recover the true amplitudes of the mass transport.

3.1.3. Winds with basin-scale curl: March 1985

The average winds of March 1985 (Fig. 11) constitute a more typical example of the winds over the GIN Sea. The negative curl corresponds to the Greenland High occupying the NW half of the basin, and the positive curl represents the average of all the winter cyclones sweeping from the Denmark Straits to occupy the southeastern half of the GIN Sea. However, unlike the high pressure region, which is almost always present with varying intensity, this region of low pressure is not permanent but rather an average of 5 or 6 lows that traverse the region at various speeds and intervals. Some of the synoptic weather patterns will be published in a follow-up report on the time-dependent simulations.
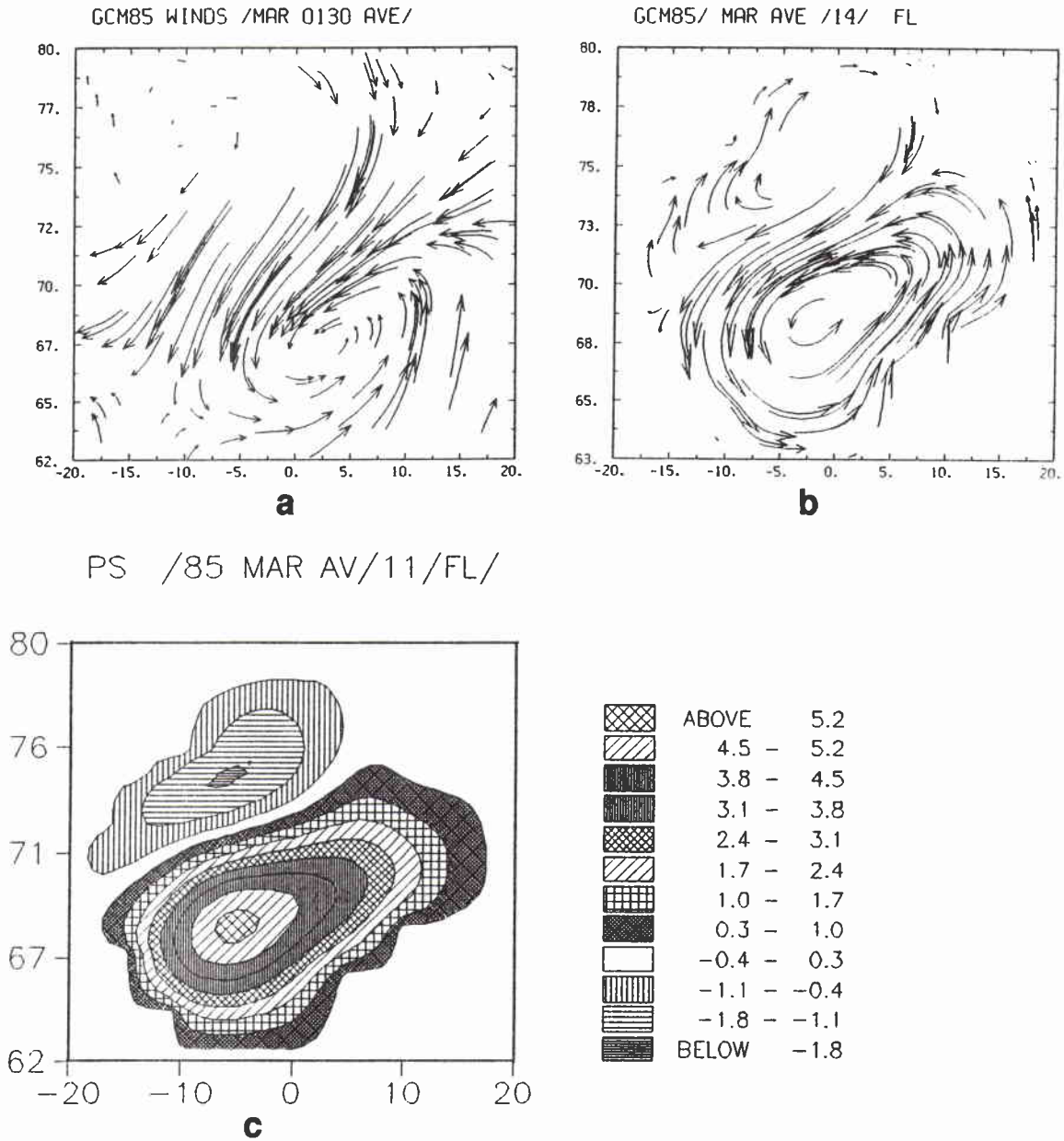
Flat bottom case   The corresponding circulation patterns computed for the flat-bottom case are shown in Figs. 11–15. The transport vectors and streamlines show a clockwise flow in the northwestern half of the basin (Fig. 11), undoubtedly associated with the Greenland high, and a strong cyclonic flow in the southeastern part of the Norwegian Sea. A comparison is made of the transport with the wind vectors which reflect the curl of the wind field. A simple correlation seems to exist between the two fields. In the northwestern region of the anti-cyclonic wind patterns, the ocean also develops an anti-cyclonic, high surface-elevation eddy. Similarly, in the southeastern region the strong cyclonic wind patterns drive a strong cyclonic, low surface elevation gyre. The areas of positive and negative curls of the wind stress and the ocean currents seem to correspond fairly well, but a discrepancy appears between the relative magnitudes. The strength of the cyclonic circulation is three times the anti-cyclonic circulation, as evidenced by the ratio Ψ_{max}/Ψ_{min} (see Fig. 12 and Table 2). The strengths of the respective wind curls, on the other hand, differ only by about 10%. One of the reasons for this discrepancy is masked by the mapping procedure employed. In reality the longitude lines converge strongly poleward in the GIN Sea area (mean latitude 70°N), so that gyres located in the upper half of the figures occupy much less area than shown. Since the stream function is essentially vorticity integrated twice in space, small differences in the peak wind curl and the area it occupies can result in much larger differences in the corresponding ocean circulation. The flat-bottom simulations bring out the effects of geometry, friction and wind curl scale, without masking by the complicated topographic interactions.

A comparison of the streamlines and surface heights in Fig. 13 again reveals almost no differences in the patterns. The respective contour lines coincide closely; the arguments given above concerning the cause of this coincidence still apply.

The results of the friction sensitivity tests are shown in Figs. 14 and 15. Each figure contains the results for four values of the lateral friction coefficient, with $A = 10$, 10^2, 10^3 and 10^4 m²/s, respectively. For $A = 10$ the solution needed 60 days to converge, and for $A = 10^4$ only 20, with the others converging between these limits. Almost no visible differences appear in the circulation patterns as defined by the wind contour arrows and the streamlines. Differences appear only in the intensity of the circulation. As expected, the strongest circulation occurs for the lowest value of A.

The overall differences between the flat bottom and GIN topography results, and between the March 1985 and December '87 calculations are shown in Tables 1 and 2. For the March '85 simulations, the flat bottom results for $|h|$ range (Table 1) from 1.81–2.85 cm for A in the range $10^4 - 10$ m²/s, respectively.

The amplitudes of the stream function $|\Psi|$ for the flat bottom simulations (Table 2) range from 3.48–5.64 $\times 10^6$ m³/s, for the friction range $10^4 - 10$ m²/s. Again, note that there is essentially no difference between the results for $A = 10$ and 10^2, and

GCM85 WINDS /MAR 0130 AVE/

GCM85/ MAR AVE /14/ FL

a

b

PS /85 MAR AV/11/FL/

⊠ ABOVE		5.2
▨ 4.5	–	5.2
▦ 3.8	–	4.5
▥ 3.1	–	3.8
▨ 2.4	–	3.1
▧ 1.7	–	2.4
▦ 1.0	–	1.7
▨ 0.3	–	1.0
☐ −0.4	–	0.3
▥ −1.1	–	−0.4
▤ −1.8	–	−1.1
▦ BELOW		−1.8

c

Figure 12 *A comparison of (a) the wind stress, (b) oceanic mass transport vectors, and (c) streamlines, for the flat bottom simulations based upon the March 1985 average winds, and a lateral friction coefficient, $A = 10^4$ m^2/s. (Streamline units are 10^6 m^3/s.)*

only about a 4% change for $A = 10^3$ m^2/s; however, the amplitude for $A = 10^4$ is down by a substantial 56%.

From the point of view of the strength of the simulated circulation, the value $A = 10^4$ may not be an acceptable one. However, if other reasons compel the use of such values (mostly numerical, as in the topographic case, described below) we must scale
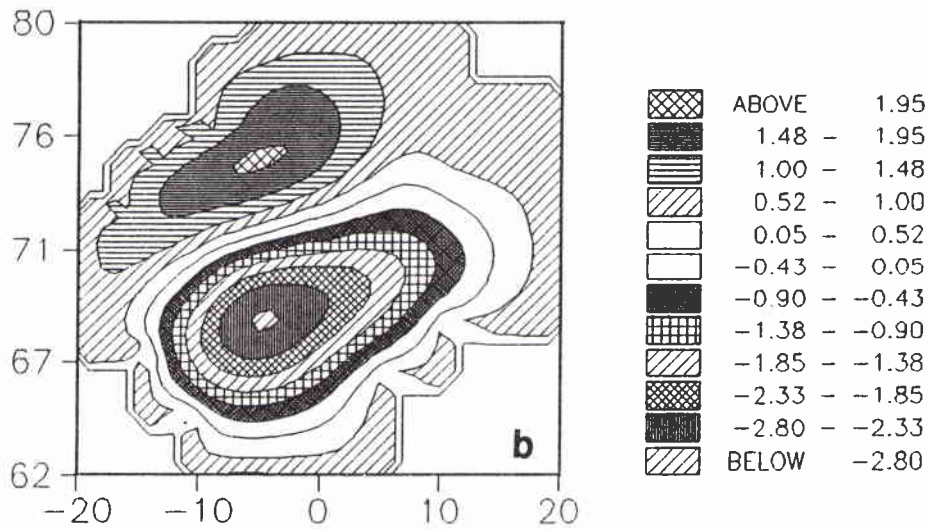
PS /85 MAR AV/11/FL/

|	
ABOVE	5.2
4.5 –	5.2
3.8 –	4.5
3.1 –	3.8
2.4 –	3.1
1.7 –	2.4
1.0 –	1.7
0.3 –	1.0
−0.4 –	0.3
−1.1 –	−0.4
−1.8 –	−1.1
BELOW	−1.8

H /85 MAR AV/11/FL/

ABOVE	1.95
1.48 –	1.95
1.00 –	1.48
0.52 –	1.00
0.05 –	0.52
−0.43 –	0.05
−0.90 –	−0.43
−1.38 –	−0.90
−1.85 –	−1.38
−2.33 –	−1.85
−2.80 –	−2.33
BELOW	−2.80
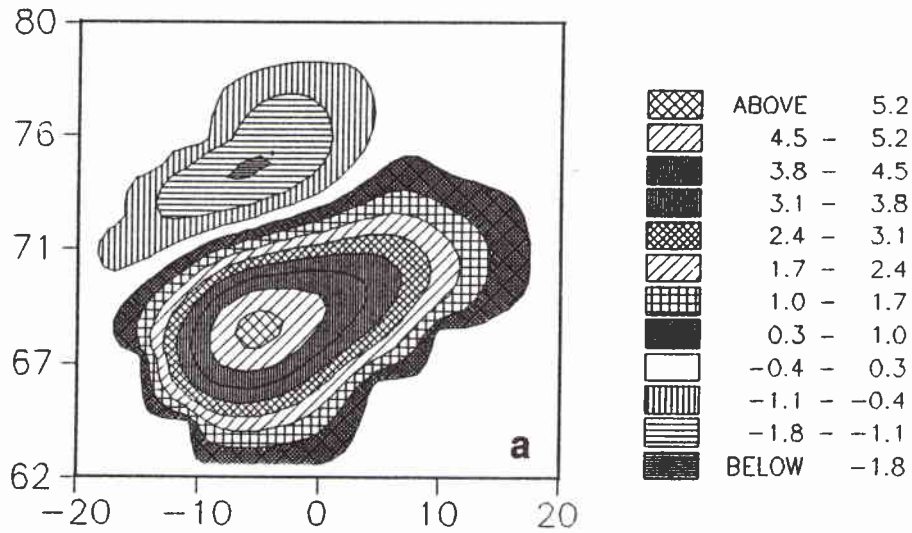
Figure 13 *A comparison of (a) streamlines, and (b) sea surface elevation contours for the flat bottom simulation of Fig. 12. (Streamline units are 10^6 m^3/s; surface elevations contour interval is in cm.)*

the magnitudes of the computed currents and surface elevation amplitudes according to the results presented in Tables 1 and 2.

GIN Sea topography case The wind vectors, current vectors and streamline patterns corresponding to the GIN Sea topography simulations with $A = 10^4$ m^2/s are
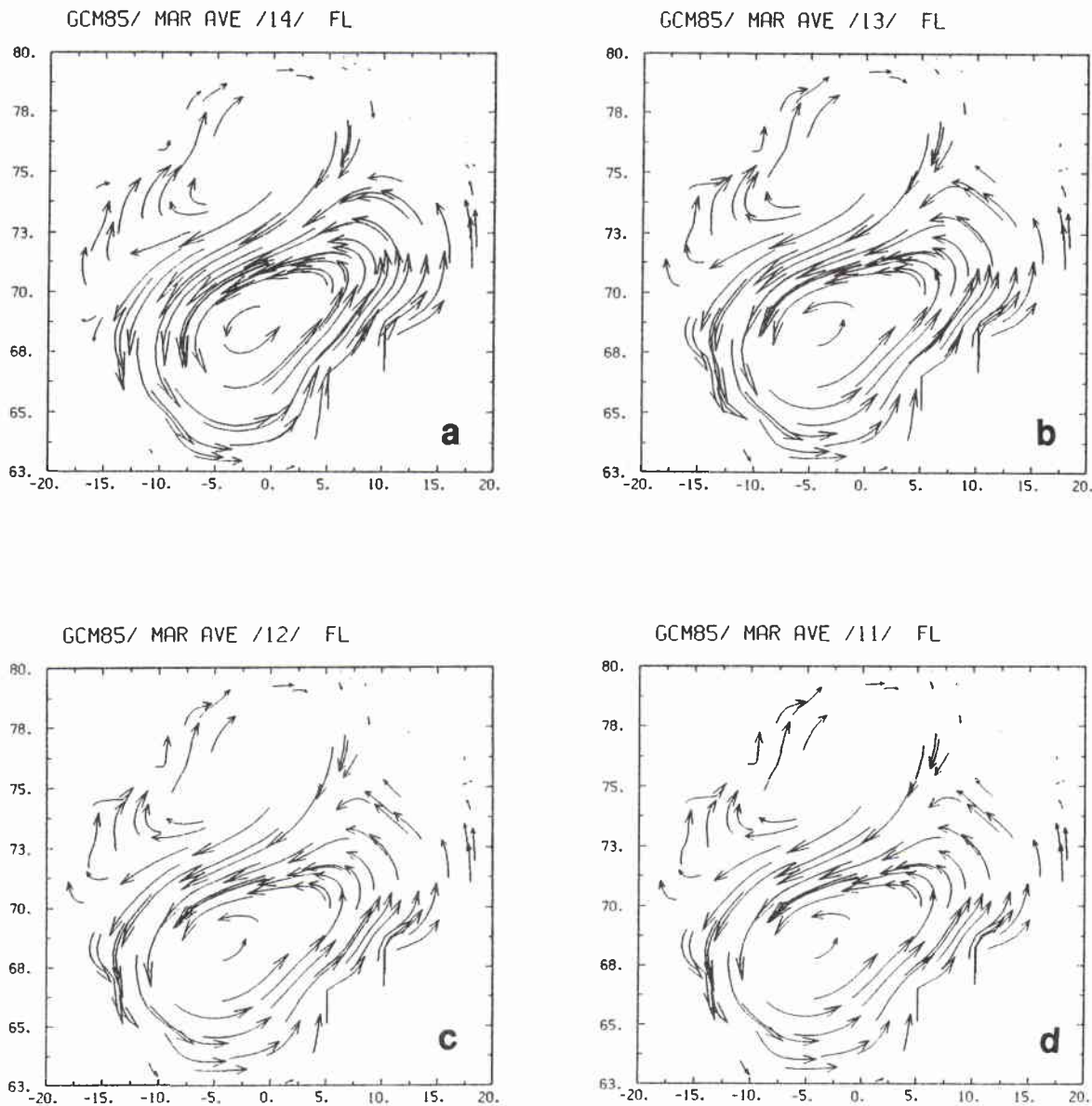
Figure 14 *The circulation forced by the March 1985 average wind stress in a flat bottom GIN Sea basin, for different values of the lateral friction coefficient A: (a) $A = 10^4$, (b) $A = 10^3$, (c) $A = 10^2$, and (d) $A = 10$ (all are in $m^2 s$).*

shown in Figs. 16 and 17. One can immediately obtain a quick overview of the effects of topography from inspecting either figure. The current vectors, to a large extent, follow the topography. The direction of the circulation still depends on the wind forcing, with an anti-cyclonic, high surface level gyre developing under the Greenland high in the northwestern part of the GIN Sea, and a strong cyclonic circulation in the southwestern part under the strong low pressure system over the Norwegian Sea. However, the exact boundaries of these gyres, the direction of their respective
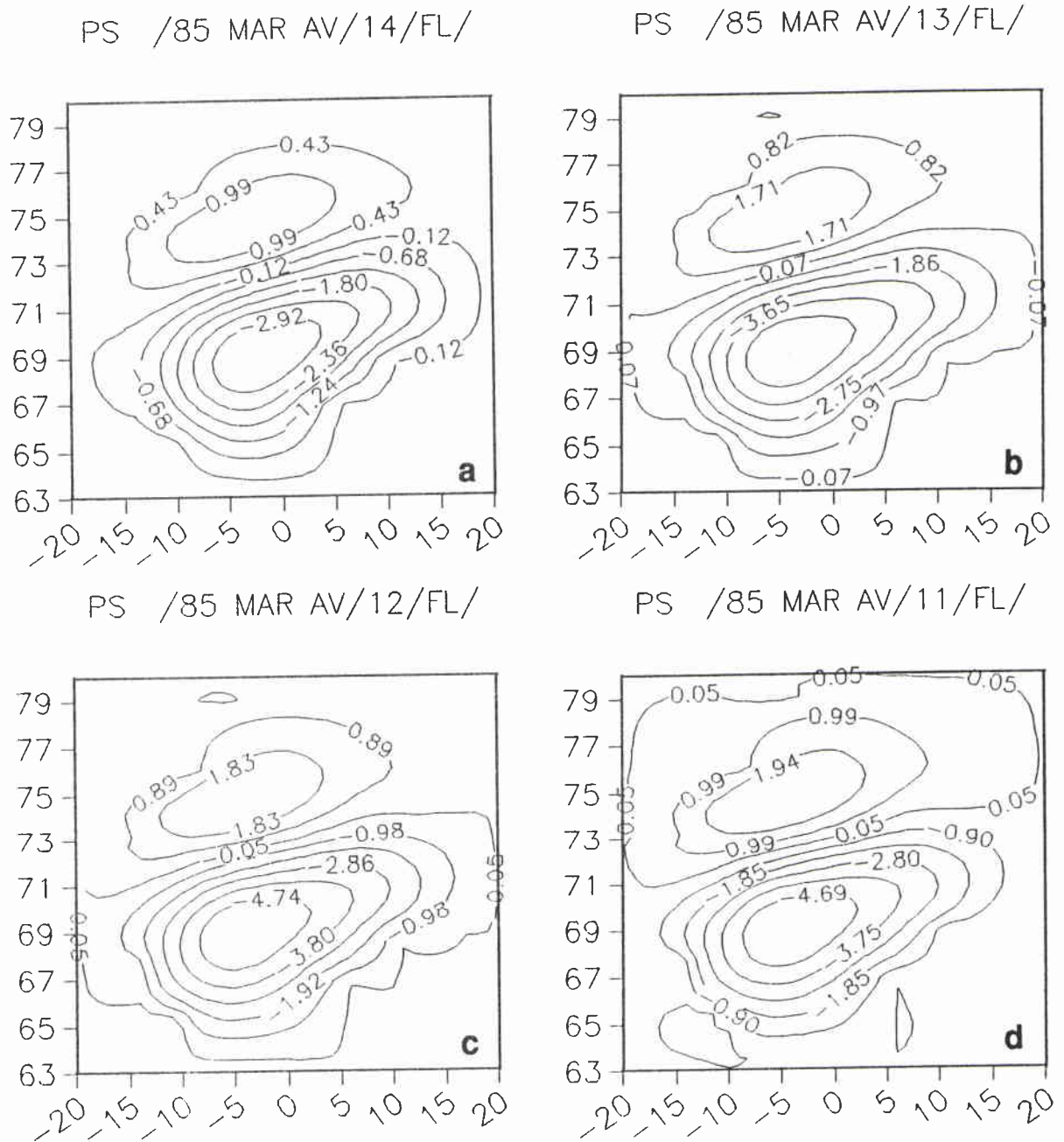
Figure 15 *The streamlines of the circulation patterns of March 1985, as a function of the lateral friction coefficient A (see Fig. 14). ((Streamline units are 10^6 m^3/s; (a) $A = 10^4$, (b) $A = 10^3$, (c) $A = 10^2$, and (d) $A = 10$.*

currents, and the strengths of the circulations are strongly influenced by the topography. A degree of correlation does exist between the wind curl and the streamlines. In a sense, there is a 'cyclonic tendency rule', that is, under the influence of cyclonic winds, cyclonic ocean currents tend to develop. Nevertheless, a quick inspection
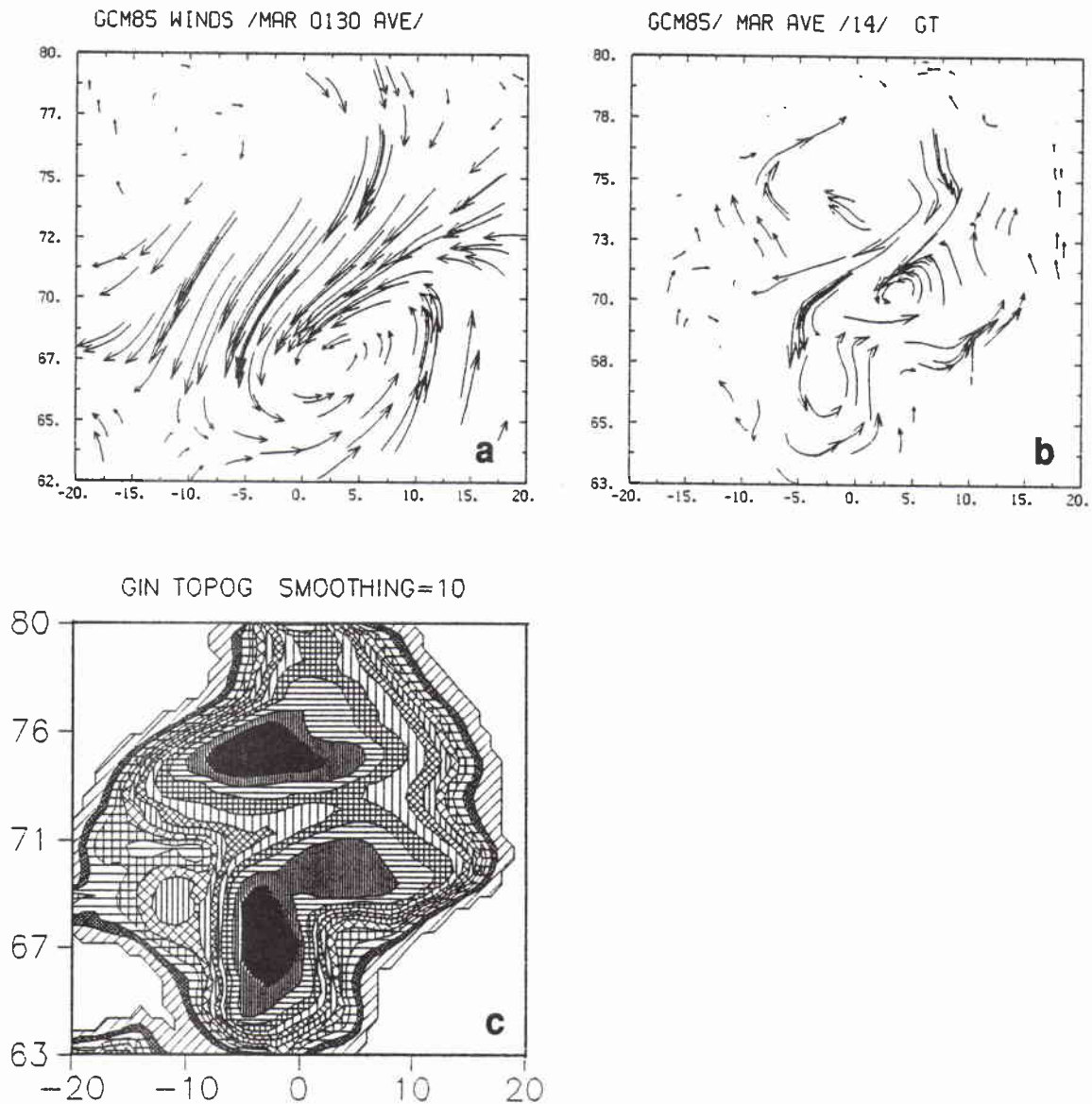
Figure 16   *The circulation forced by the March 1985 monthly mean wind stress, using the GIN Sea topography given in Fig. 1 and the lateral friction coefficient $A = 10^4$ m^2/s: (a) wind stress vectors, (b) mass transport vectors, and (c) topographic contours. (See Fig. 1 for scale.)*

demonstrates the parallelism between the streamlines and topographic contours.

The only noticeable exception to this cyclonic tendency (associated with a depression) is a region adjoining the Barents Sea, where the water seems to pile up to a level equal to about half the maximum depression over the Norwegian Sea. This is somewhat surprising in view of the fact that the prevailing winds in that region
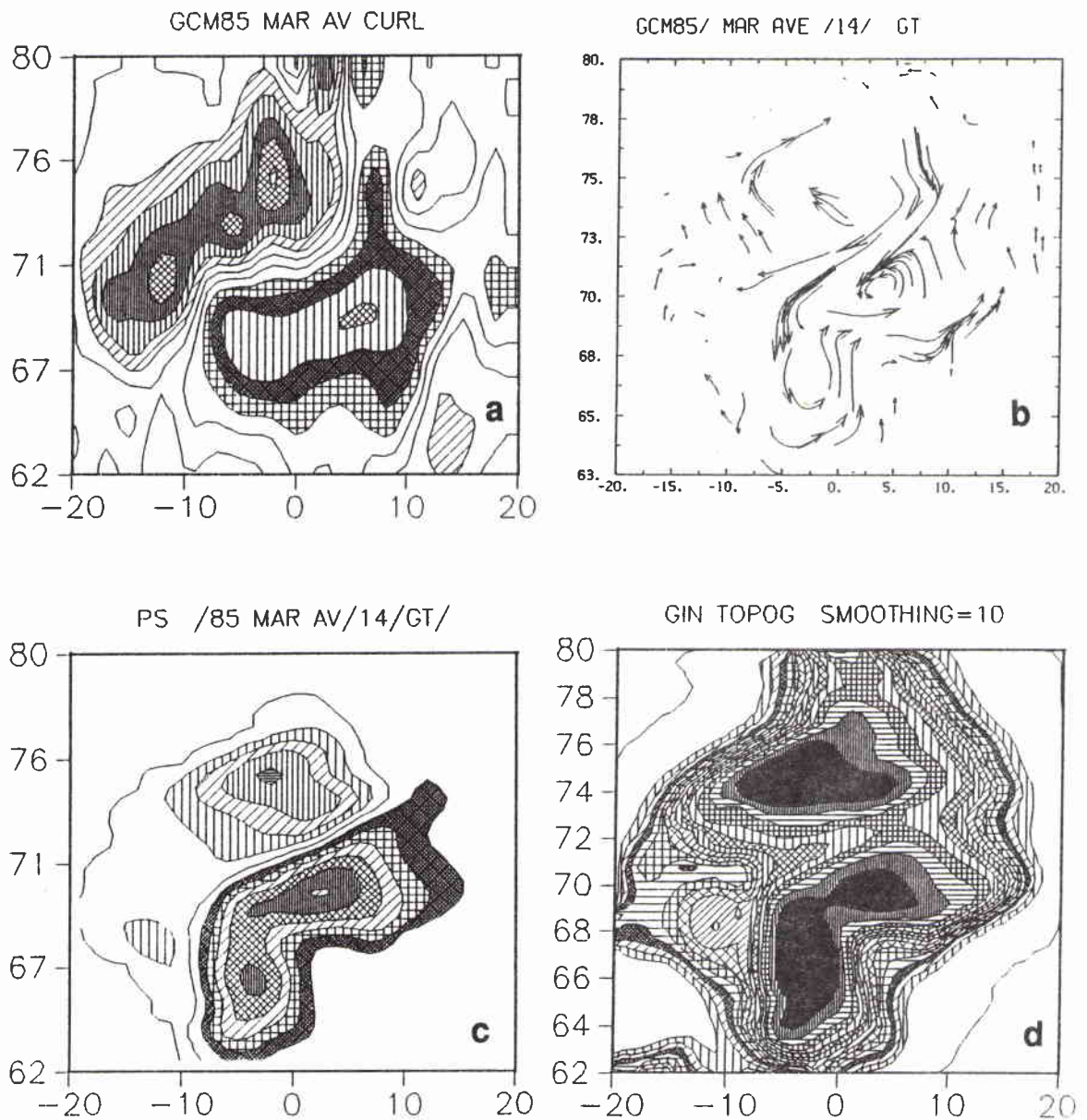
Figure 17 *The March 1985 circulation of Fig. 16 with the wind curl and streamline contours added: (a) wind curl, (b) mass transport vectors, (c) mass transport streamlines, and (d) smoothed topography (see Fig. 1 for scale). (Curl units are 10^{-6} m/s; streamline units are 10^6 m^3/s.)*

blow into the GIN Sea, so that their direct forcing effect would be to push water away from the boundary and into the GIN Sea. This can be partially explained by a northward moving jet that exists near the boundary in that region, and which requires a positive (east-west) elevation gradient for maintenance by geostrophy.

As in the flat-bottom simulations, we have investigated the effect of the lateral friction coefficient A upon the circulation. These results are presented in Figs. 18–20. Each of these figures contains the results for four values of the lateral friction coefficient, with $A = 10^4$, 10^3, 10^2 and 10 m^2/s. For $A = 10^4$ m^2/s the solutions look smooth like in the flat bottom simulations, but for $A = 10^2$ and $A = 10$ the stream function plots contain progressively increasing noise. The height fields tend to remain smooth even for those values of the lateral friction, indicating that it is the interaction of the vorticity field with the topography that introduces noise into the system. The percentage changes between the $|\Psi|$ maxima for $A = 10$, 10^2, 10^3 and 10^4 are 4%, 12% and 43%, respectively, based on the value for $A = 10$. We can thus perform simulations comfortably with lateral friction coefficient values up to 10^3 or so, before the actual magnitude of the solutions is appreciably reduced.

Again, we make an instructive comparison between contours of the mass transport and the surface elevation (Fig. 21). Surprisingly, even in the presence of topography, there is a high degree of parallelism of the respective contour lines.

3.1.4. Winds with coherent small-scale curl: the December 1987 winds

For this test we have chosen the average 1987 December winds. These winds and their corresponding curl pattern are shown in Fig. 22. They show a basically northerly flow down to about 66°N, with enough curvature in the streamlines to reveal the presence of the high pressure area over Greenland (anti-cyclone), and a low pressure area over the Barents Sea. There is also a strong convergence zone present in the latitude belt 62–66°N, which deflects the northerly flow to the west and east, respectively, about the 0° meridian. The curl field reveals a large anti-cyclonic area over Greenland, corresponding to the well-known Greenland high climatological pressure feature, and a small but strong cyclonic area between Norway and Spits-bergen. There are several smaller irregular features, among them an anticyclone that apparently is connected to the Greenland High, and another less intense low over the Norwegian Sea. However, although the total areas occupied by cyclonic and anti-cyclonic wind motions are similar to those in the March 1985 case, the areas of intense activity are restricted to more numerous but much smaller areas; the net result is much less wind curl available for driving the ocean circulation. In this case there appear to be two high pressure centers and four or five low pressure centers, though only two of them are of high intensity.

Flat bottom experiments   The wind vectors, mass transport vectors, and the mass transport streamline contours for this case are presented in Fig. 23. The December 1987 circulation displays a much more distinctive single-gyre pattern than the March 1985 results (Fig. 11); over 80% of the GIN Sea basin is occupied by a strong cyclonic gyre. Only a small anti-cyclonic gyre, centered on 71°N,15°W next to Greenland, breaks up the complete dominance of the cyclonic gyre. There also appears to be a small, distinct cyclonic gyre superposed on the large one in its east-central part,
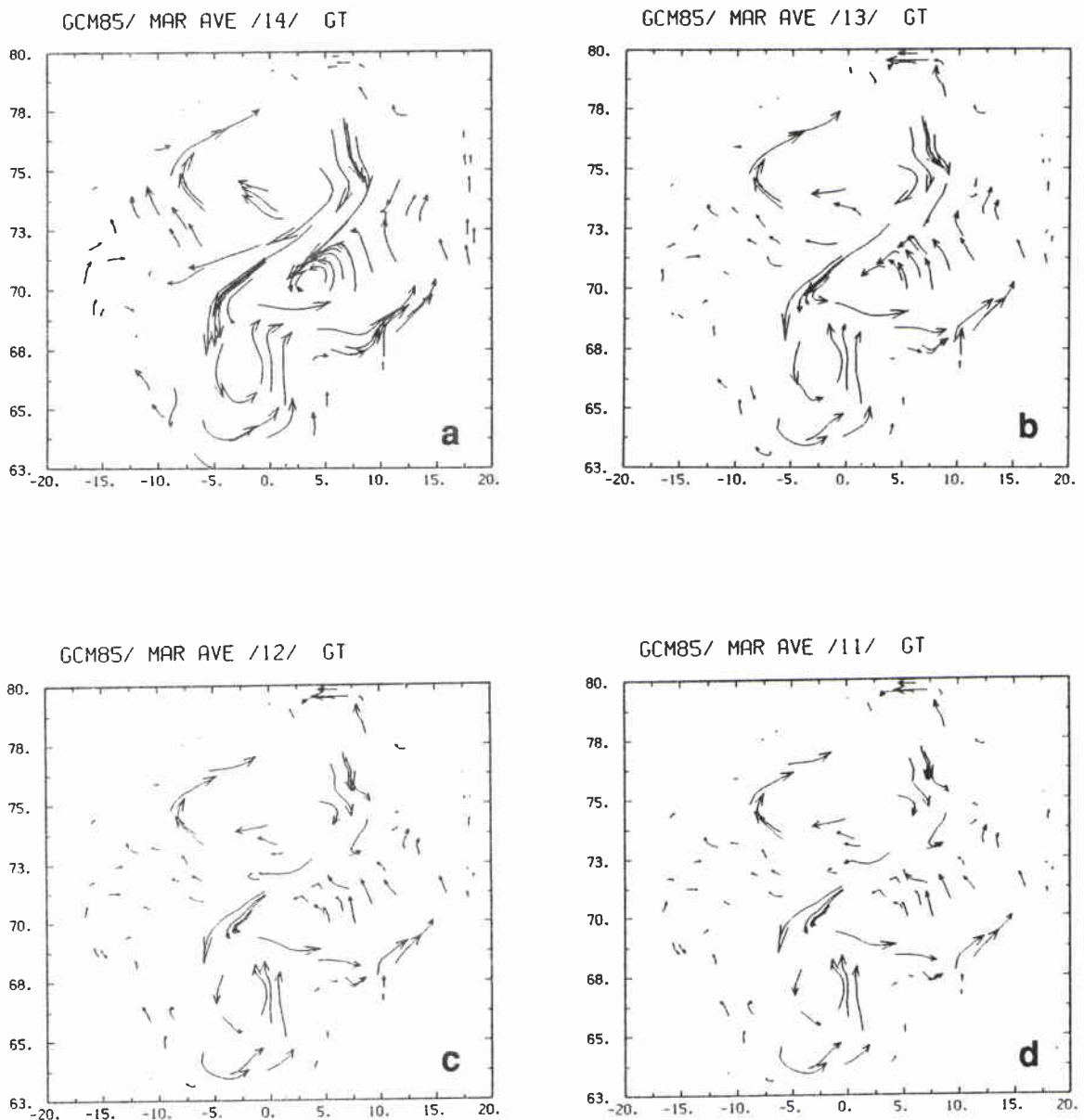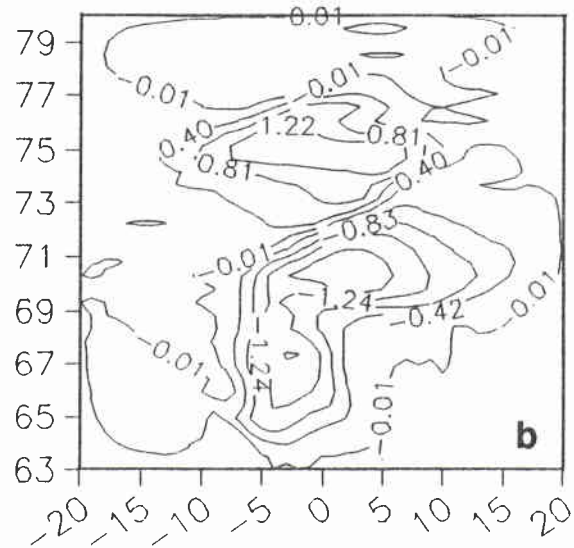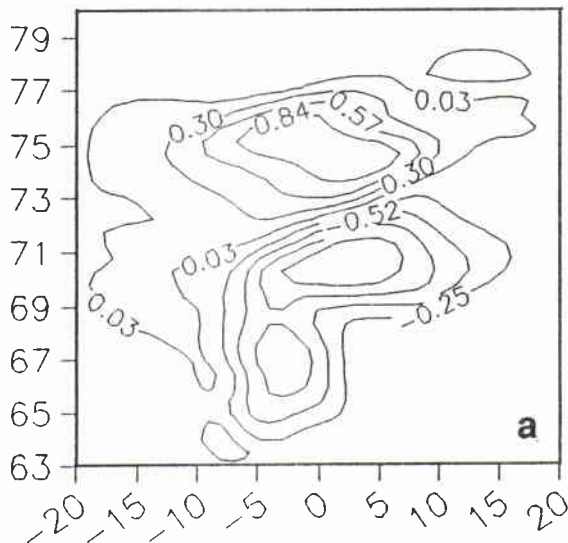
Figure 18 *The effect of horizontal friction on the March 1985 circulation with smoothed topography, for different values of the lateral friction coefficient A: (a) A = 10⁴, (b) A = 10³, (c) A = 10², and (d) A = 10.*

centered on 73°N,8°E. The peak amplitude $|\Psi|_{max}$ of the cyclonic motion is twice that of anticyclonic gyre. Both smaller-scale eddies, that is, the western anti-cyclonic gyre and the superposed eastern cyclonic gyre, become more prominent for larger values of the lateral friction coefficient. These are most evident in the mass transport vector diagram (Fig. 23b).
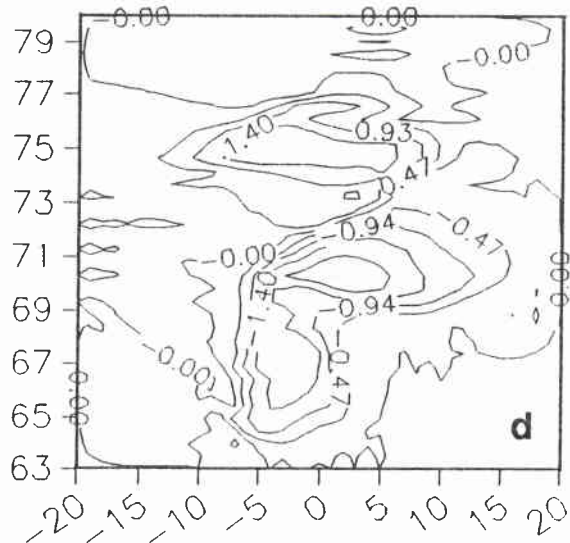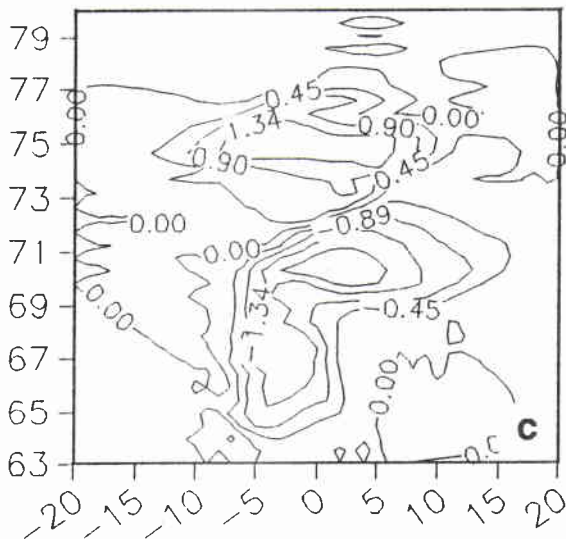
Figure 19 *The mass transport streamlines corresponding to the circulations depicted in Fig. 18 for different values of the lateral friction coefficient A: (a) $A = 10^4$, (b) $A = 10^3$, (c) $A = 10^2$, and (d) $A = 10$. (Steamline units are 10^6 m^3/s.)*
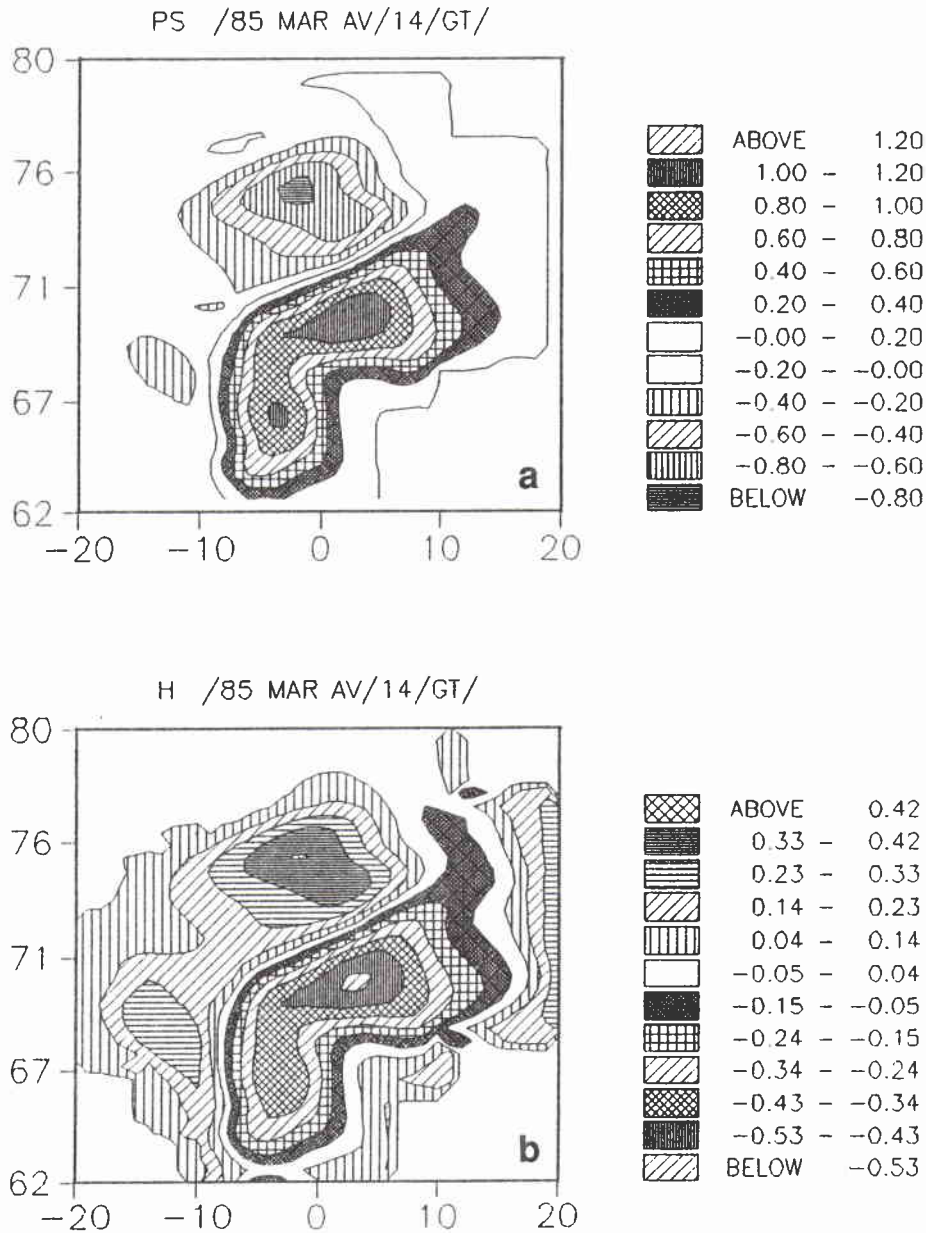
The frictional dependence of the flat bottom circulation has also been investigated; overall the same insensitivity to the value of A has been found as in the September 1965 and March 1985 simulations, with a few exceptions. Figures 24 and 25 display

H /85 MAR AV/14/GT/

H /85 MAR AV/13/GT/

H /85 MAR AV/12/GT/

H /85 MAR AV/11/GT/
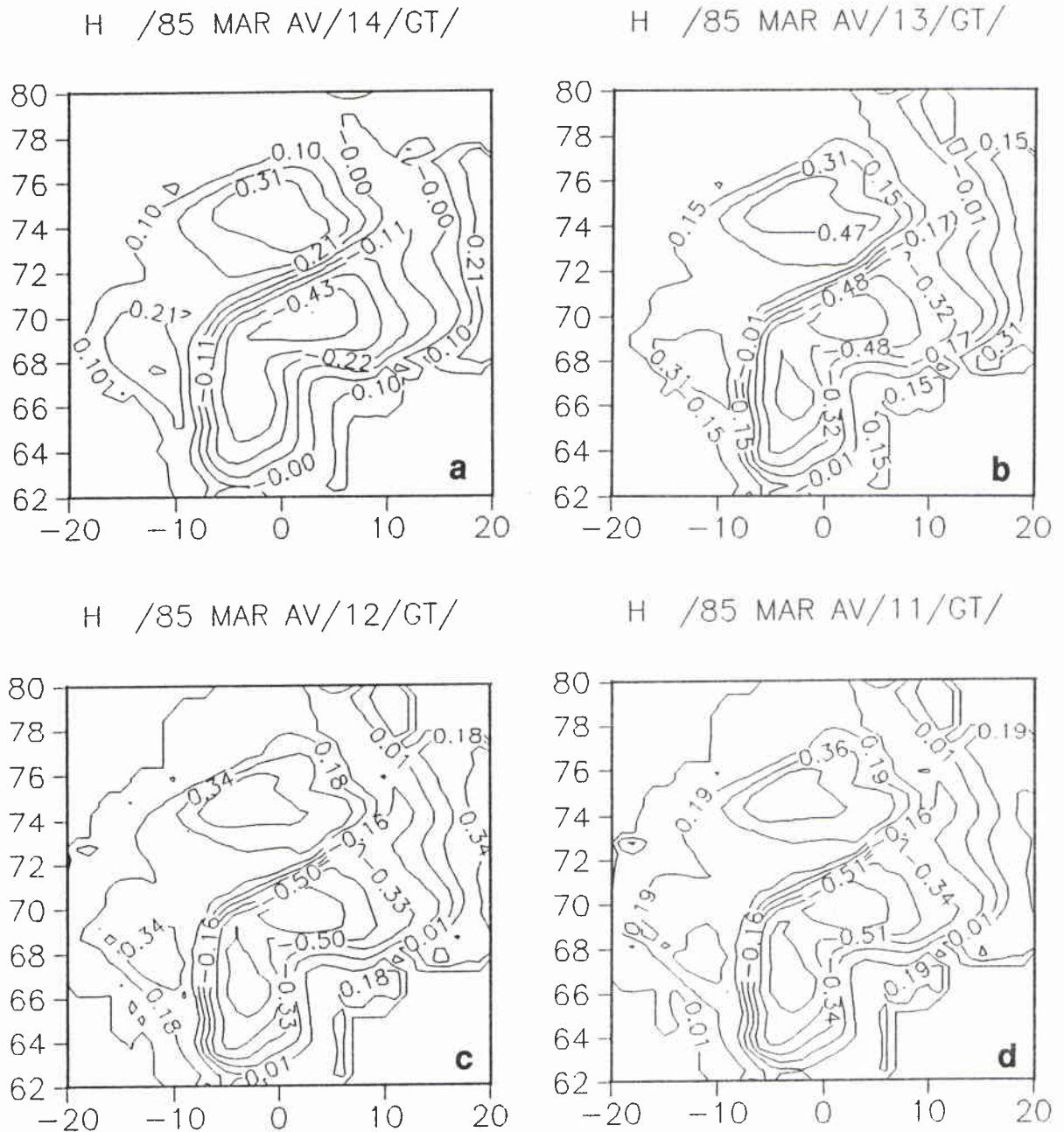
Figure 20 *The surface elevation for the March 1985 topographic circulation as a function of the different lateral friction coefficients. (a) $A = 10^4$, (b) $A = 10^3$, (c) $A = 10^2$, and (d) $A = 10$. (Surface elevations is in cm.)*

the mass transport vectors and mass stream lines, respectively. A noteworthy feature is a marked decrease of the anti-cyclonic cell east of Greenland for $A = 10^2$ m^2/s, based on changes seen in the mass transport streamlines displayed in Fig. 24. Almost the opposite conclusion can be reached on inspecting Fig. 23, because the 'arrow

PS /85 MAR AV/14/GT/

	ABOVE	1.20
	1.00 –	1.20
	0.80 –	1.00
	0.60 –	0.80
	0.40 –	0.60
	0.20 –	0.40
	–0.00 –	0.20
	–0.20 –	–0.00
	–0.40 –	–0.20
	–0.60 –	–0.40
	–0.80 –	–0.60
	BELOW	–0.80

H /85 MAR AV/14/GT/

	ABOVE	0.42
	0.33 –	0.42
	0.23 –	0.33
	0.14 –	0.23
	0.04 –	0.14
	–0.05 –	0.04
	–0.15 –	–0.05
	–0.24 –	–0.15
	–0.34 –	–0.24
	–0.43 –	–0.34
	–0.53 –	–0.43
	BELOW	–0.53

Figure 21 *A comparison of the (a) streamlines and (b) surface elevation contours for the March 1985 flat bottom simulation of Fig. 18. (Streamline units in 10^7 m^3/s; surface elevation contour interval is 10 cm.)*

contours' indicate that this anti-cyclonic gyre is in fact strongest for the $A = 10$ m^2/s value. In these diagrams one can also detect the presence of a small, tight anti-cyclonic gyre embedded into the eastern half of the large cyclonic gyre; this again is strongest for $A = 10^4$ and essentially disappears for $A = 10$ m^2/s. The best way to reconcile these two conclusions is to remember that:
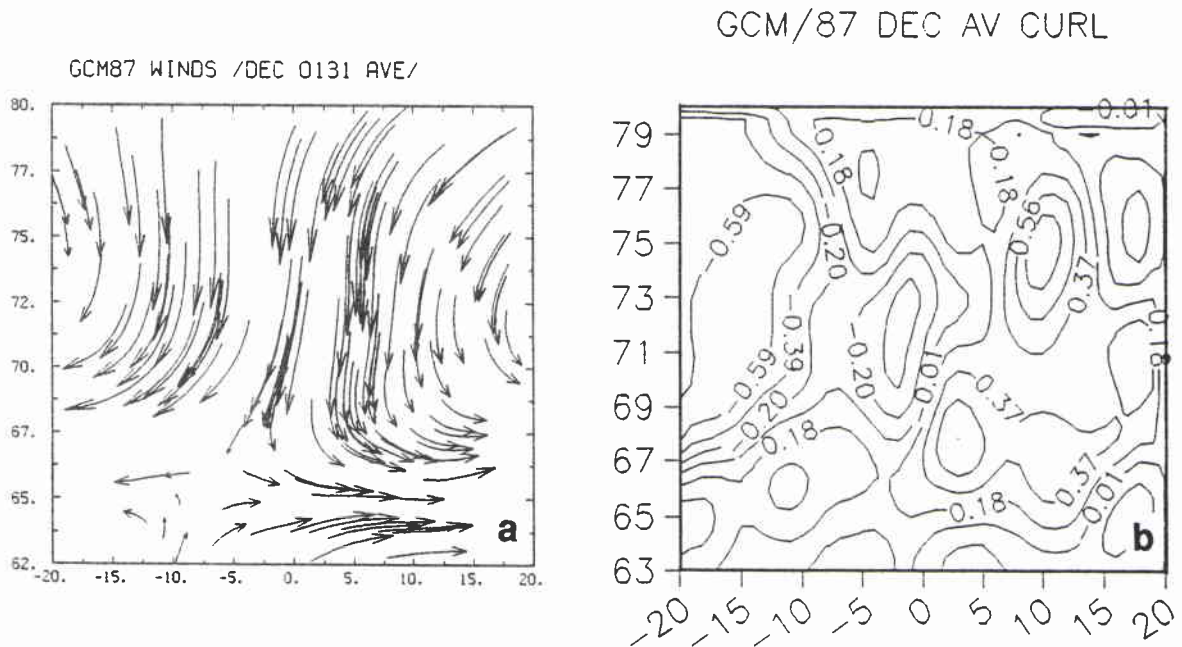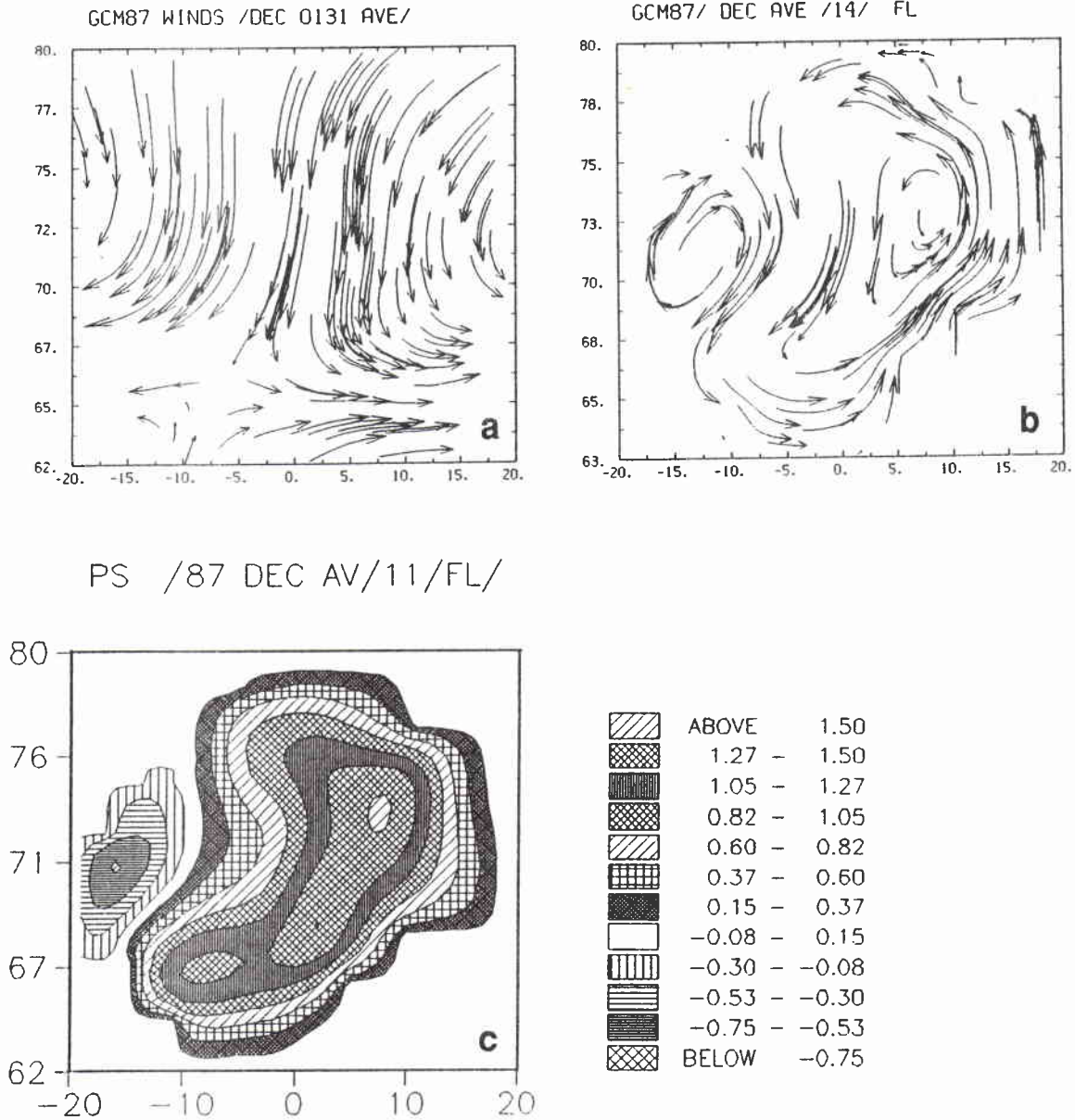
Figure 22 *The December 1987 (a) average wind stress field and (b) its curl. (Curl units are 10^{-6} m/s.)*

(a) For small values of A, the flow is more chaotic to which the arrows are much more sensitive than the streamlines, which represent twice integrated vorticity in space.

(b) The arrows represent the total velocity field, not just the non-divergent component of it (this latter represented by the curl in the stream function).

As we have found, the March 1985 winds, the closing of the GIN Sea openings have the most severe effects at the mouths of the Barents and the Arctic Seas; the mouths restrict flows that apparently tend to exit there. Instead of exiting, these flows then form both strong jets parallel to the boundaries, and part of an overall cyclonic circulation that eventually forms a jet moving southward along the northern coast of Greenland. The main flow feature appears to be a strong jet passing north along the Norwegian coast, which being unable to exit into the Barents Sea moves northward, and eventually westward at the closed Fram Strait. Here it begins to move southward along Greenland where it forms part of the general cyclonic circulation. Thus the main effect of varying the lateral friction coefficient A is to change the intensity of the flow, with relatively weak effects on the circulation patterns.

The topographic experiments Figure 26 displays the circulation pattern for the $A = 10^4$ m^2/s case, along with the wind vectors and the smoothed topography. This circulation is dominated by a very strong, tight cyclonic gyre centered on 5°E,70°N, and bounded on the southwest and northwest by two somewhat weaker cyclonic gyres centered on 3°W,67°N and 5°W,75°N, respectively. The drastic effect of the topography is clearly evident, with the flow generally following the topography contours; however, in places where it cuts across them with sharp turns there are

Figure 23   *A comparison of (a) wind stress, (b) oceanic mass transport vectors, and (c) streamlines, for the flat bottom simulation, using the December 1987 average winds and a lateral friction coefficient value of $A = 10^2$ m^2/s. (Streamline units are $10^7 m^3/s$.)*

strong local concentrations of the wind curl. The general direction of the circulation is primarily determined by the direction of the wind curl in the respective areas of the GIN Sea basin.

The effect of the lateral friction are presented in Figs. 27 and 28. In these cases the role of A is again immediately clear, and one begins to appreciate the analytic
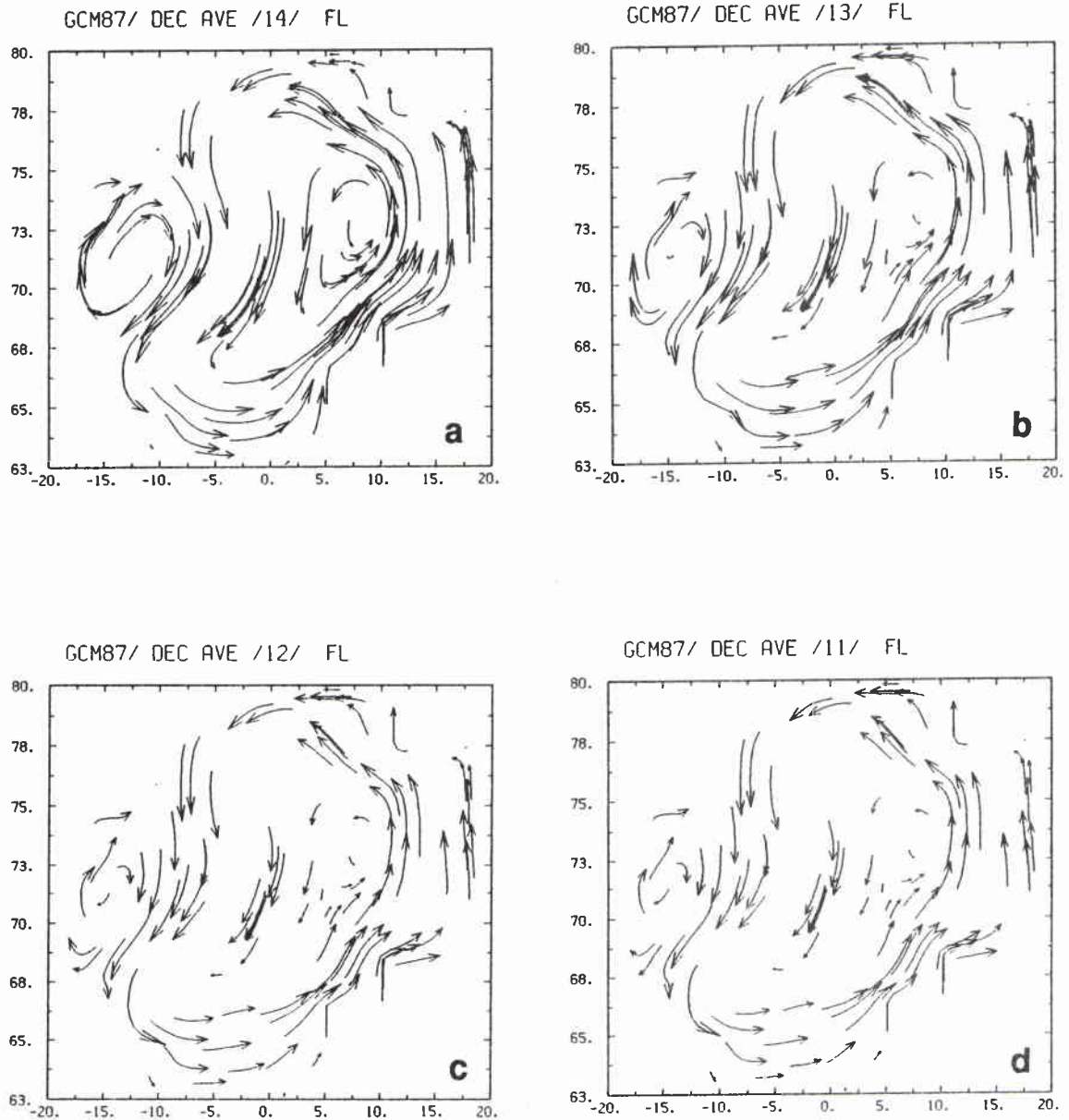
Figure 24 *The circulation forced by the December 1987 average wind stress in a flat bottom GIN Sea basin, for different values of the lateral friction coefficient A: (a) $A = 10^4$, (b) $A = 10^3$, (c) $A = 10^2$, and (d) $A = 10$.*

considerations of Sect. 2 concerning a desirable value of A in the presence of sharp topography. For $A = 10^4$ the circulation consists of three or four well-developed cyclonic gyres, whereas the circulation for $A = 10$, exhibits almost no recognizable, coherent eddy-like flow patterns. Again we see that having conservative finite difference schemes in a fluid dynamical simulation does not prevent the solution from degenerating into chaos with the same total energy! This problem becomes
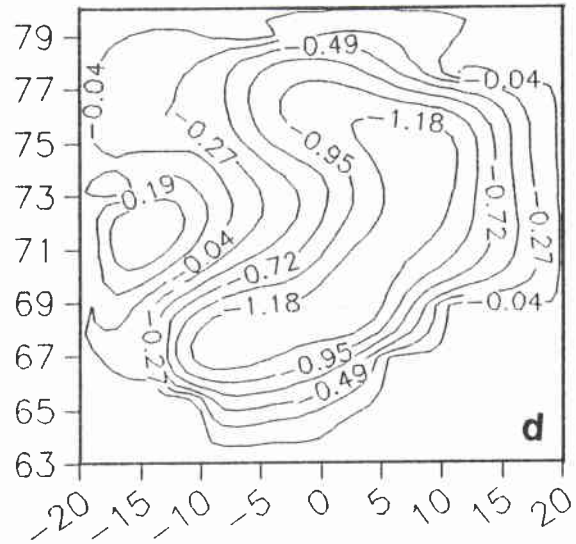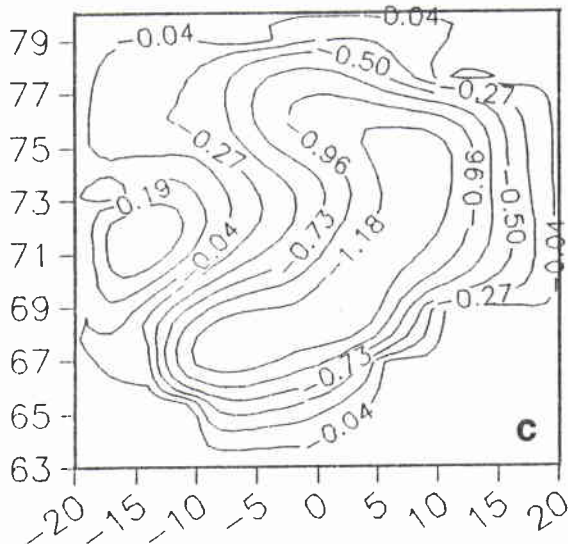
PS /87 DEC AV/14/FL/

PS /87 DEC AV/13/FL/
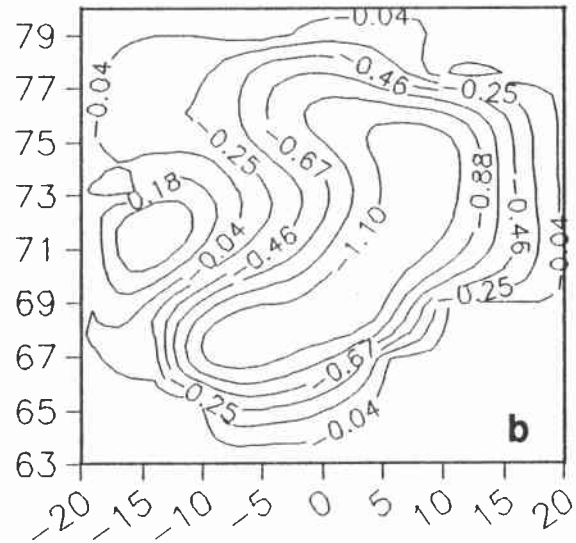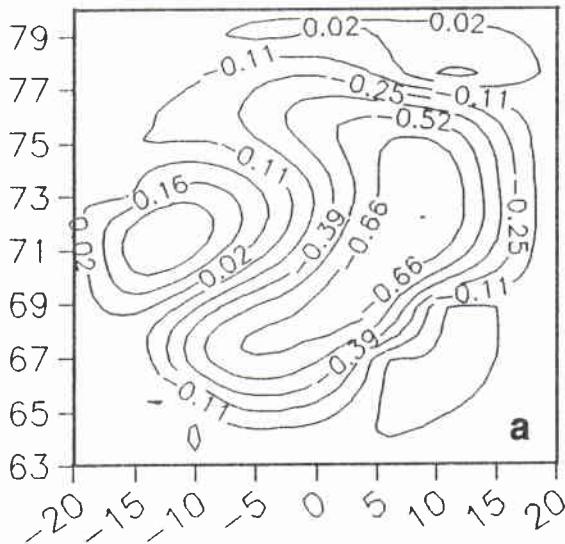
PS /87 DEC AV/12/FL/

PS /87 DEC AV/11/FL/

Figure 25 *The mass transport streamlines of the December 1987, circulation patterns (depicted in Fig. 24), as a function of the lateral friction coefficient A. (Streamline units are 10^7 m^3/s.)*

particularly acute for simulations of flows with strong nonlinearities or spatially-varying forcing (in this case topography or wind). If either the physical process of energy cascade through the nonlinear terms is modelled incorrectly, or there is an
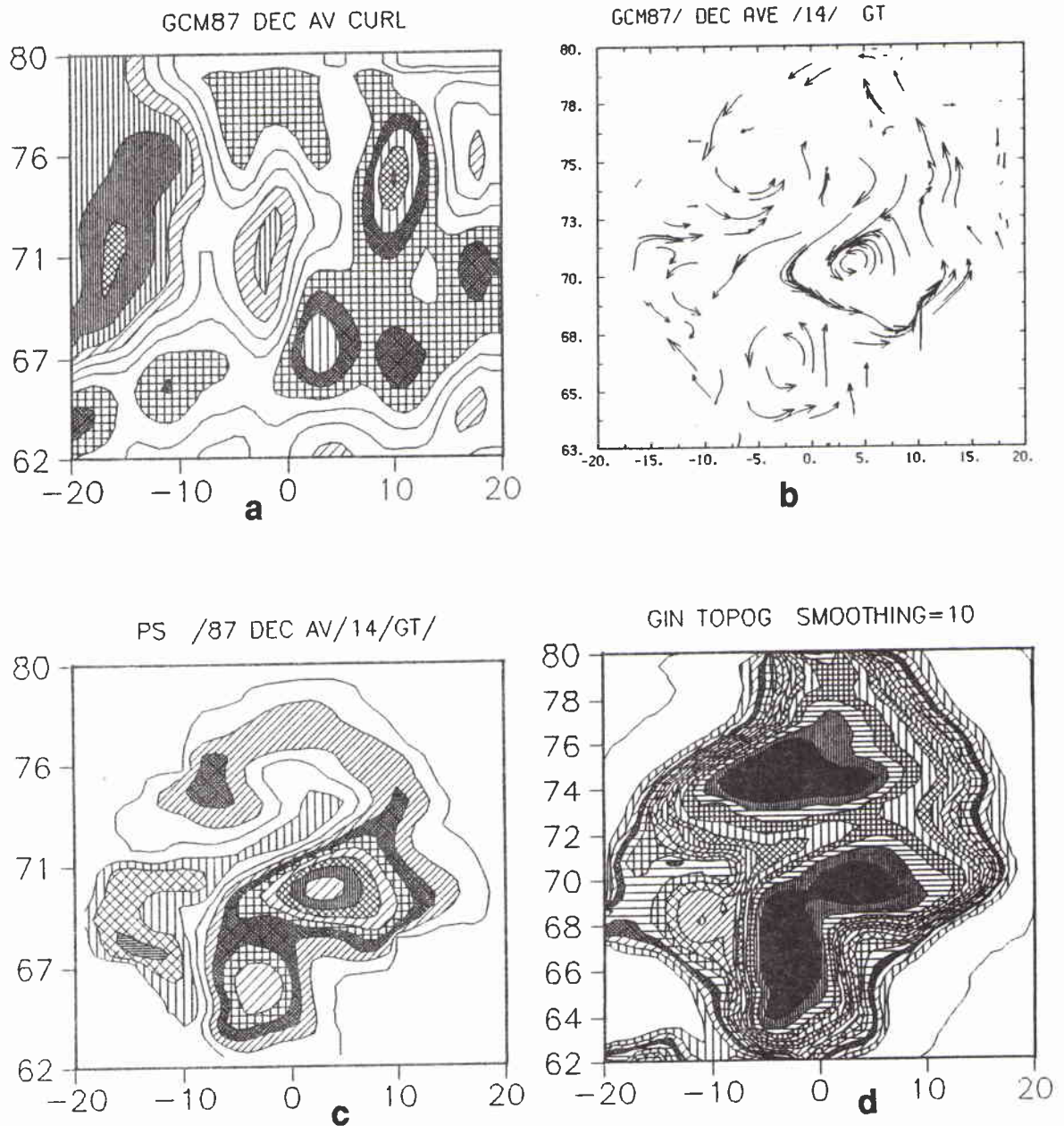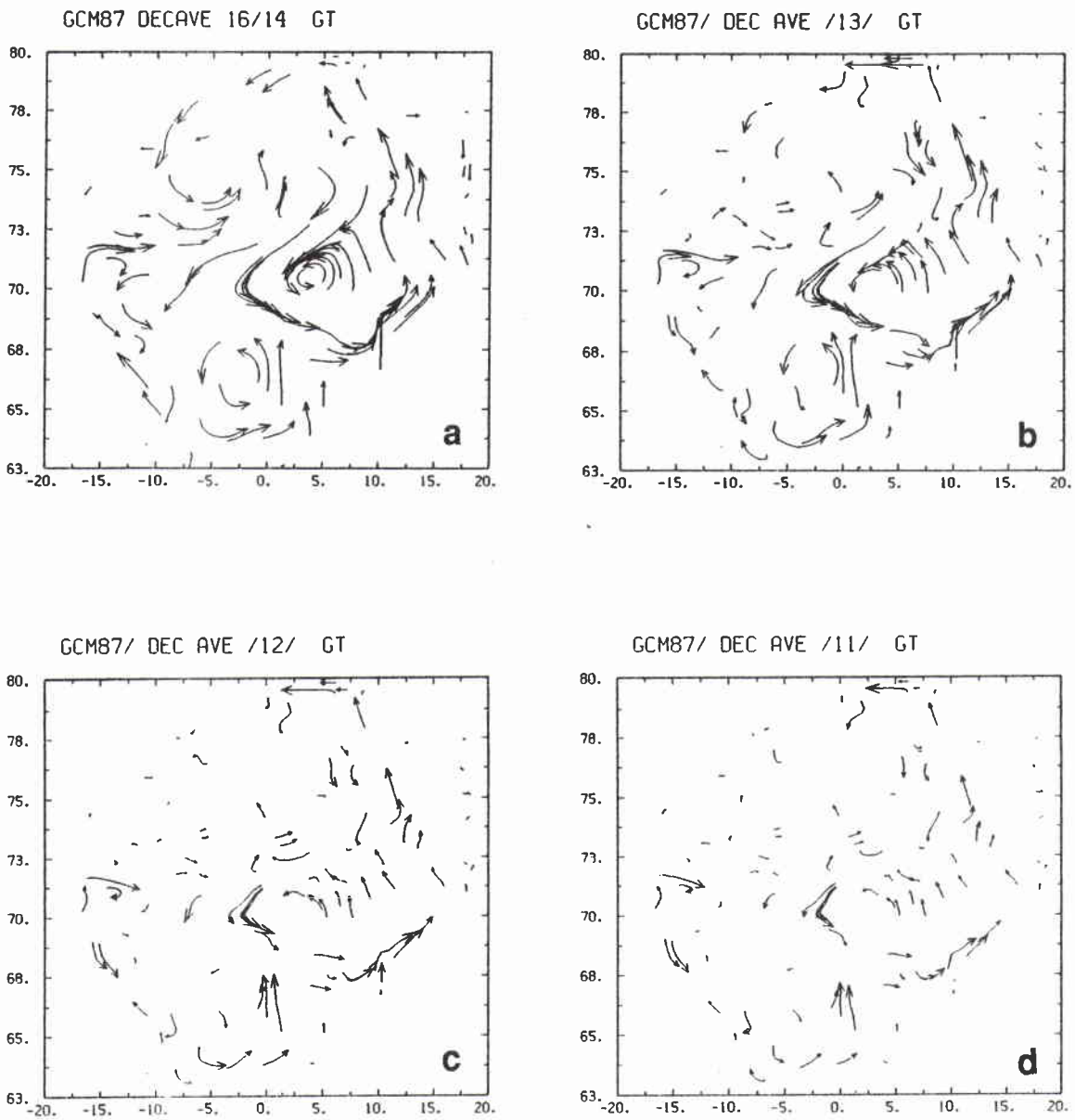
Figure 26 *The December 1987 circulation in the presence of topography: (a) wind curl, (b) mass transport vectors, (c) mass transport streamlines, (d) topographic contours (see Fig. 1 for scale). (Curl units are 10^{-6} m/s; streamline units are 10^7 m³/s.)*

inadequate spatial resolution of the forcing (topography, winds, etc.), the solution generally degenerates into chaos unless a large enough value of the lateral friction is used to act as a sink for the small-scale, irregular features which would otherwise dominate the solution. Topography appears to have a much more drastic effect on the mass transport vectors and streamlines than on the surface deviation, validating the known complexity of topography–vorticity interactions in such flows.

GCM87 DECAVE 16/14   GT

GCM87/ DEC AVE /13/   GT

GCM87/ DEC AVE /12/   GT

GCM87/ DEC AVE /11/   GT
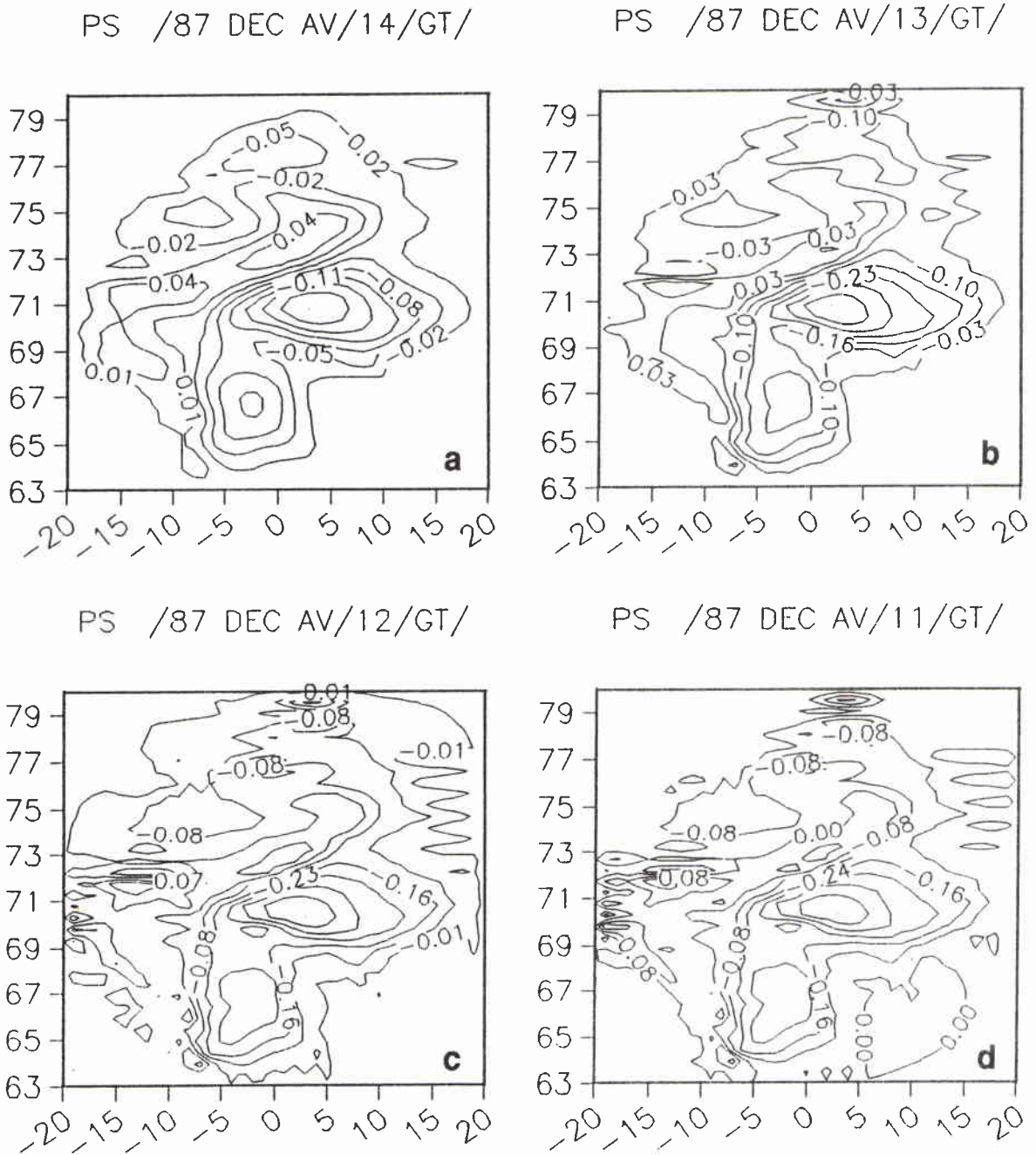
Figure 27   *The effect of horizontal friction on the December 1987 circulation with smoothed topography, for different values of the lateral friction coefficient A: (a) $A = 10^4$, (b) $A = 10^3$, (c) $A = 10^2$, and (d) $A = 10$.*

PS /87 DEC AV/14/GT/

PS /87 DEC AV/13/GT/

PS /87 DEC AV/12/GT/

PS /87 DEC AV/11/GT/

Figure 28 *The mass transport streamlines corresponding to the December 1987 circulations depicted in Fig. 27, for different values of the lateral friction coefficient A: (a) $A = 10^4$, (b) $A = 10^3$, (c) $A = 10^2$, and (d) $A = 10$.*

4

Summary and conclusions

We have developed a time-dependent barotropic model for the GIN Sea, presenting the preliminary tests that used both steady winds and closed ports. The main findings are summarized as follows:

1. Topography is the principal factor in determining the barotropic circulation in the GIN Sea. Though the general sense of the circulation follows the curl of the wind stress, the scales of gyres and eddies and the magnitudes of the transports, overwhelmingly depend on the depth and horizontal scales of the topography. Similarly, the local direction of the currents is determined mainly by the topographic contour lines.

2. The magnitude of the lateral friction used to generate stable and smooth solutions again depends on topography. With a flat bottom, lateral friction coefficients as low as $A' < 10$ m^2/s, or even lower, suffice. However, with a topography smoothed by a ten-fold application of a diffusive filter, a value of $A = 10^4$ m^2/s was needed to generate solutions without any 'noise' (i.e. unrealistic oscillations with wavelengths of $2\delta x$), even though a value of $A = 10^2$ m^2/s was sufficient to stabilize the solutions for more than 60 days. We have traced the difficulty with the topography to the term involving $g\nabla H \nabla h$, where the spatially varying 'velocity' $\sqrt{g\delta H}$ acts in a quasi-nonlinear manner in causing advective instabilities. Such effects have been found by Phillips in his first attempts at weather prediction in the late fifties and early sixties.

3. The circulations generated in the southern half of the basin by the winds of September '65, December '87 and March '85, were found to be very similar, consisting of a cyclonic gyre with two vorticity maxima corresponding to the two sub-basins. On the other hand, the circulations generated in the northern half of the basin were different. The September and December cases show a cyclonic circulation, with southerly currents along the Greenland coast; these reinforce the otherwise omnipresent East Greenland Current which is mostly baroclinic in nature. On the other hand, the March circulation consists of an anti-cyclonic gyre with northerly currents along the Greenland coast; these then oppose and weaken the predominant East Greenland Current. In all cases, a fairly strong barotropic jet moves in a southwesterly direction along the Jan Mayen ridge.

References

[1] Creegan, A. A numerical investigation of the circulation in the Norwegian Sea. *Tellus*, **28**, 1976: 451–459.

[2] Legutke, S. The influence of boundary conditions on the circulation in the Greenland–Norwegian Sea: A numerical investigation. *In:* Nihoul, J.C.J. and Jamart, B.M. *eds.* Three-dimensional models of marine and estuarine dynamics. Amsterdam, Elsevier, 1987: 269–283.

[3] Aagaard, K. Wind-driven transports in the Greenland and Norwegian Seas. *Deep-Sea Research*, **17**, 1970: 281–291.

[4] Stevens, D. A three-dimensional primitive equation model of the Norwegian and Greenland Seas. Paper presented at the EGS Meeting, Bologna, Italy, 22–25 March 1988.

[5] Suenderman, J. and Lenz, W. *eds.* North Sea Dynamics. Berlin, Springer, 1983.

[6] Nowlin, W.D. A steady, wind-driven, frictional model of two moving layers in a rectangular ocean basin. *Deep-Sea Research*, **14**, 1967: 89–110.

[7] Davies, A.M. Application of a three-dimensional shelf model to the calculation of North Sea currents. *In:* Suenderman, J. and Lenz, W., *eds.* North Sea Dynamics. Berlin, Springer, 1983: 44–62.

[8] Soetje, K.C. and Brockmann, An operational numerical model of the North Sea and the German Bight. *In:* Suenderman, J. and Lenz, W., *eds.* North Sea Dynamics. Berlin, Springer, 1983: 95–107.

[9] Davies, A.M. and James, I.D. Three-dimensional Galerkin-spectral sea models of the North Sea and German Bight. *In:* Suenderman, J. and Lenz, W., *eds.* North Sea Dynamics. Berlin, Springer, 1983: 85–94.

[10] Backhaus, J.O. and Maier-Reimer, E. On seasonal circulation in the North Sea. *In:* Suenderman, J. and Lenz, W., *eds.* North Sea Dynamics. Berlin, Springer, 1983: 63–84.

[11] Durance, J.A. and Hughes, D.G. Experiments with two- and three-dimensional numerical models of the north-east coast of England. *In:* Suenderman, J. and Lenz, W., *eds.* North Sea Dynamics. Berlin, Springer, 1983: 120–133.

[12] Roache, P.J. Computational Fluid Dynamics. Albuquerque, N.M., Hermosa Publishers, 1972.

[13] Flather, R.A. and Proctor, R. Prediction of North Sea storm surges using numerical models: recent developments in the UK. *In:* Suenderman, J. and Lenz, W., *eds.* North Sea Dynamics. Berlin, Springer, 1983: 299–317.

[14] Furnes, G.K. Wind effects in the North Sea. *Journal of Physical Oceanography*, **10**, 1980: 978–984.

[15] Grammeltvedt, A. A survey of finite-difference schemes for the primitive equations for a barotropic fluid. *Monthly Weather Review*, **97**, 1969: 384–404.

[16] Bryan, K. A numerical method for the study of the circulation of the world ocean. *Journal of Computational Physics*, **4**, 1969: 347–376.

[17] Navon, I.M. and de Villiers, R. Application of the Turkel-Zwas explicit large time-step scheme to a hemispheric barotropic model with constraint restoration. *Monthly Weather Review*, **115**, 1987: 1036–1051.

[18] Schoenstadt, A.L. Transfer function analysis of numerical schemes used to simulate geostrophic adjustment. *Monthly Weather Review*, **108**, 1980: 1248–1259.

[19] Wu, J. Wind-stress coefficients over sea surface from breeze to hurricane. *Journal of Geophysical Research*, **87**, 1982: 9704–9706.

[20] Liu, W.T., Katsaros, K.B. and Businger, J.A. Bulk parametrization of air-sea exchanges of heat and water vapor including the molecular constraints at the interface. *Journal of Atmospheric Science*, **36**, 1979: 1722–1735.

Initial Distribution for SM-242

SCNR for SACLANTCEN		_National Liaison Officers_	
SCNR Belgium	1	NLO Canada	1
SCNR Canada	1	NLO Denmark	1
SCNR Denmark	1	NLO Germany	1
SCNR Germany	1	NLO Italy	1
SCNR Greece	1	NLO Netherlands	1
SCNR Italy	1	NLO UK	1
SCNR Netherlands	1	NLO US	4
SCNR Norway	1		
SCNR Portugal	1		
SCNR Spain	1		
SCNR Turkey	1	**Total external distribution**	26
SCNR UK	1	SACLANTCEN Library	10
SCNR US	2	Stock	24
SECGEN Rep. SCNR	1		—
NAMILCOM Rep. SCNR	1	**Total number of copies**	60